A STUDY ON DEVELOPMENT OF MACHINABLE CALCIUM PHOSPHATE BASED BIO-COMPOSITES WITH ZIRCONIA, BORON OXIDE AND LANTHANUM OXIDE

A THESIS SUBMITTED TO
THE GRADUATE SCHOOL OF NATURAL AND APPLIED SCIENCES
OF
MIDDLE EAST TECHNICAL UNIVERSITY

BY

SINA KHOSHSIMA

IN PARTIAL FULLFILLMENT OF THE REQUIREMENTS
FOR
THE DEGREE OF MASTER OF SCIENCE
IN
BIOMEDICAL ENGINEERING

JANUARY 2015

Approval of the Thesis

A STUDY ON DEVELOPMENT OF MACHINABLE CALCIUM PHOSPHATE BASED BIO-COMPOSITES WITH ZIRCONIA, BORON OXIDE AND LANTHANUM OXIDE

submitted by **SINA KHOSHSIMA** in partial fulfillment of the requirements for the degree of **Master of Science in Biomedical Engineering Department, Middle East Technical University** by,

Prof. Dr. Gülbin Dural Ünver _____
Dean, Graduate School of **Natural and Applied Sciences**

Prof. Dr. Vasıf Hasırcı _____
Head of Department, **Biomedical Engineering**

Assoc. Prof. Dr. Zafer Evis _____
Supervisor, **Engineering Sciences Dept., METU**

Assist. Prof. Dr. Metin Özgül _____
Co-supervisor, **Materials Science and Engineering Dept., Afyon Kocatepe University**

Examining Committee Members:

Prof. Dr. Kadri Aydınol _____
Metallurgical and Materials Engineering Dept., METU

Assoc. Prof. Dr. Zafer Evis _____
Engineering Sciences Dept., METU

Assoc. Prof. Dr. Ayşen Tezcaner _____
Engineering Sciences Dept., METU

Assoc. Prof. Dr. Senih Gürses _____
Engineering Sciences Dept., METU

Assist. Prof. Dr. M. Tolga Yılmaz _____
Engineering Sciences Dept., METU

Date: 27.01.2015

I hereby declare that all information in this document has been obtained and presented in accordance with academic rules and ethical conduct. I also declare that, as required by these rules and conduct, I have fully cited and referenced all material and results that are not original to this document.

Name, Last name: Sina Khoshsima
Signature:

ABSTRACT

A STUDY ON DEVELOPMENT OF MACHINABLE CALCIUM PHOSPHATE BASED BIO-COMPOSITES WITH ZIRCONIA, BORON OXIDE AND LANTHANUM OXIDE

Khoshsima, Sina

M. Sc., Department of Biomedical Engineering

Supervisor: Assoc. Prof. Dr. Zafer Evis

Co-Supervisor: Assist. Prof. Dr. Metin Özgül

January 2015; 97 Pages

The aim of this study was to investigate the microstructure, mechanical and biological properties of pure hydroxyapatite and composites of hydroxyapatite with zirconia, boron oxide and lanthanum oxide. Hydroxyapatite was synthesized via precipitation method and sintered at 1100°C for 1 h. It was observed that relative density of the sintered composites including zirconia was increased while the density of composites including boron oxide decreased. For physical and structural analysis, X-ray diffraction, scanning electron microscopy, energy dispersive X-ray spectroscopy, mercury intrusion porosimetry and Fourier transform infrared spectroscopy examinations were performed. Due to boron oxide and zirconia substitution, small amounts of β-TCP phase were detected besides hydroxyapatite. Scanning electron microscopy results revealed that addition of composite powders resulted in smaller grains for zirconia group and bigger grain size for boron oxide group. Presence of different atoms and their corresponding weight ratios were determined by energy dispersive X-ray spectroscopy. Mercury intrusion porosimetry test showed the percent porosity of the composites. In Fourier transform infrared spectroscopy analysis, in

addition to the characteristic bands of hydroxyapatite, novel bands indicating the substitution of zirconia, boron oxide and Lanthanum oxide were observed in samples. The microhardness test revealed that zirconia had a positive effects on the mechanical properties of the samples up to a certain amount, while substitution of the boron oxide had a negative effect on their mechanical properties. In order to evaluate the biocompatibility, in vitro cytotoxicity tests were performed using Saos-2 cells. PrestoBlue® assay viability test was used to analyze cell proliferation on the surface of samples. It was observed that composites including zirconia have a better biocompatibility and higher cell attachment rate than those including boron oxide. Scanning electron microscopy images were examined to observe morphology of the cells on the surface of the samples and it was observed that in all samples, the surface of the pellets were covered with cell layers showing perfect cell-material interaction.

Keywords: Hydroxyapatite, Zirconia, Boron oxide, Lanthanum oxide, Mechanical properties, Biocompatibility.

ÖZ

ZİRKONYA, BOR OKSİT VE LANTANYUM OKSİT İLAVE EDİLMİŞ KALSİYUM FOSFAT BAZLI İŞLENEBİLİR BİYOKOMPOZİTLERİN GELİŞTİRİLMESİ ÜZERİNE BİR ÇALIŞMA

Khoshsima, Sina

Yüksek Lisans, Biyomedikal Mühendisliği Bölümü

Tez Yöneticisi: Doç. Dr. Zafer Evis

Yardımcı Tez Yöneticisi: Yrd. Doç. Dr. Metin Özgül

Ocak 2015; 97 Sayfa

Bu çalışmanın hedefi saf hidroksiapatit ve zirkonya, bor oksit ve lantanum oksit içeren hidroksiapatit kompozitlerin mikroyapı, mekanik ve biyolojik özelliklerinin incelenmesidir. Hidroksiapatit, çöktürme metoduyla sentezlenmiş ve 1100°C'de bir saat boyunca sinterlenmiştir. Bor oksit içeren kompozitlerin yoğunluk miktarı azalırken zirkonya içeren sinterlenmiş kompozitlerin göreceli yoğunluğu artmıştır. Fiziksel ve yapısal analiz için X-ışını kırınımı, taramalı electron mikroskobu, enerji dağılımlı X-ışını spektroskopi, cıva intrüzyon porozimetri ve kızıl ötesi spektroskopi incelemeleri yapılmıştır. Bor oksit ve zirkonyanın yer değişiminden dolayı, β-TCP fazı az miktarlarda hidroksiapatit'in yanında gözlemlenmiştir. Taramalı electron mikroskob sonuçları, kompozit tozların eklenmesinin zirkonya grubunda daha küçük boyutta taneciklere neden olduğunu göstermişken, bor oksit grubunda daha büyük boyutta taneciklere neden olduğunu göstermiştir. Farklı atomların varlığı ve bunların ağırlık oranları enerji dağılımlı X-ışını spektroskopi ile bulunmuştur. Cıva intrüzyon porozimetri testi kompozitlerin porozite yüzdesini göstermiştir. Kızıl ötesi spektroskopi analizinde, hidroksiapatitin karakteristik şeritlerine ek olarak zirkonya, bor oksit ve lantanyum oksit yer değişimini belirten yeni şeritler örneklerde

gözlemlenmiştir. Mikrosertlik testi, zirkonya'nın belirli bir miktara kadar örneklerin mekanik özelliklerine olumlu katkısı olduğunu gösterirken, bor oksit'in yer değişiminin örneklerin mekanik özelliklerine olumsuz katkısı olduğu görülmüştür. Biyouyumluluğu değerlendirmek için, örneklere deney ortamında Saos-2 hücreleri kullanılarak sitotoksisite testleri yapılmıştır. PrestoBlue® yaşayabilirlik testi örneklerin yüzeyinde hücre artışının analizi için kullanılmıştır. Zirkonya içeren kompozitlerde daha iyi biyouyumluluk ve bor oksit içerenlere göre daha yüksek hücre bağlanma oranı gözlemlenmiştir. Taramalı electron mikroskobundan alınan görüntüler, örneklerin yüzeyindeki hücrelerin morfolojilerinin incelenmesi için kullanılmıştır. Bütün örneklerde, numunelerin yüzeylerinin kusursuz hücre-malzeme etkileşimine sahip hücre katmanlarıyla kaplı olduğu gözlemlenmiştir.

Anahtar Kelimeler: Hidroksiapatit, Zirkonya, Bor oksit, Lantanyum oksit, Mekanik özellikler, Biyouyumluluk.

ACKNOWLEDGMENTS

Before all else, I would like to express my outmost gratefulness and appreciation to my advisor Assoc. Prof. Dr. Zafer Evis for his sacrifices, patience and guidance throughout this study. I learnt a lot of precious life experiences from him, and benefited from his fascinating vast knowledge. He gave me the encouragement, direction, precision and discipline I need to become a better person, and I cannot thank him enough.

I present my sincerest gratitude to my co-advisor Assist. Prof. Dr. Metin Özgül, whose guidance, support and concern helped me complete this thesis, especially in SEM, XRD, EDX, mercury intrusion porosimetry and FTIR studies.

I would also like to acknowledge Assoc. Prof. Dr. Ayşen Tezcaner for her precious guidance and time, support and patience throughout the in vitro studies.

I owe my sincerest thanks and regards to my lab friend and mentor, Aydin Tahmasebifar, for his guidance during my experiments and patience with my lack of experience. I owe a great share of what I learnt, if not all, to him. I also would like to express my outmost respect and gratitude to Dr. Bengi Yılmaz, who supervised me throughout the biological experiments of this thesis, despite her extremely busy schedule. I also would like to recognize my dear friend and mentor, Dr. Ayşegül Kavas, who thought me morals and patience in academic path.

I would like to express my deepest thankfulness to my dearest friend and brother, Serhat Özdemir, who was with me each and every step of the way till the end, and helped me beyond words in my sad and down days, when you get to know your real friends. He taught me what is now my life motto: ‘In vino veritas, in aqua sanitas’. I cannot thank him enough, and it is

my honor to be his friend.

I also want to thank my dear friends and roommates, Fatih Yılmaz, Orhan Ata Bayman, Gökhan Elmas, Dr. Ali Charkhesht, Dr. Farzin G. Golzar, Saber Hafez Qorani, Mustafa Usman, Dr. Cavid Shiriyev, Kelly Buis, Araz Cabbarlı, Nuri Akhundov, Çağri Çavdaroğlu, Ali Afshar and Armin Nabizadeh for their precious friendship. They were my family here in Turkey all along the way, stood by me in my bad and good days, and supported me constantly. They mean more than friends to me.

Finally and above all, I would like to give my greatest thanks to my parents Parviz Khoshsima and Fatemeh Hemmatzadeh and my little sister Ayda, for the values they taught me and the endless support they provided through my entire life. I would not be who I am or where I am in my life without them. They endured with me and more than me, all along the way and I owe everything to them. I do not believe that I can thank them for their sacrifices. I just want to say that I know and I understand and I really appreciate it. I love you with all my heart and I hope I made you proud.

TABLE OF CONTENTS

LIST OF TABLES

TABLES

LIST OF FIGURES

FIGURES

CHAPTER 1

INTRODUCTION

1.1 General

Bone is a tissue which possess high self-repair and regeneration potential, however, if the defect that needs to be bridged or healed is too large, the fracture might not come together on its own and eventually lose function [1,2]. This issue has made presence of metals or ceramics to help heal such defects essential. Although these ceramics and metals are being widely used to improve the healing process of bone defects, producing a scaffold that is close to bone in terms of morphology, mechanical properties and biocompatibility all together remains a challenge [3,4]. Hydroxyapatite (HA), since it's the main constituent of the bone minerals, has been widely used to produce composite materials that can assist bone defect healing process or be used as an implant which bone tissue can grow into, but since it has inferior mechanical properties, mixing it with other powder materials, such as zirconia (ZrO_2) , boron oxide (B_2O_3) or lanthanum oxide (La_2O_3), to form a bio-composite which satisfies both mechanical and biological properties of the implant has been an interest field for many scientists [5,6,7,8].

In this study, composites of HA with ZrO_2, B_2O_3 and La_2O_3 were synthesized in different weight compositions and their structural, physical, mechanical and biological properties were investigated. Density measurements, XRD, SEM, FTIR, EDX and mercury intrusion porosimetry tests were conducted to investigate different structural and physical properties of the samples. To study the mechanical properties of the samples, micro-hardness, diametral tensile strength and drilling tests were also

done. Viability and SEM tests were conducted to investigate the biocompatibility of the synthesized composites and to study morphology of cells seeded on the samples.

This thesis is consisted of four chapters. In chapter one, a brief introduction regarding to bone, materials used in this study and their mechanical and biological properties are given. Second chapter covers the definition and description of various methods used. In third chapter, results and discussions regarding to experiments conducted on composites are presented. Finally, chapter four includes a brief conclusion of the results obtained throughout the thesis.

1.2 Apatite

Apatites are a family of chemical compounds with phosphotic bases which have a similar hexagonal shape and their structure shapes according to the general chemical formula $X_{10}(YO_4)_6Z_2$. 'Apatites are widely distributed as accessory minerals in igneous rocks and in small quantities in most metamorphic rocks' [9]. The constitutive raw material is the phosphate rock (microcrystalline apatite), those of biological origin, are mainly composed of carbonated fluorapatite. It is the basic material for phosphate fertilizer manufacture and is widely used in chemical industry for the production of many different merchandises like detergents, dentifrices, plasticizers, rust removers and pharmaceuticals [9,10]. Since the material's lattice is very permissive on ionic substitutions, vacancies and solid solutions, various ions can be substituted into its structure. Table 1.1 represents a summary of these ions.

Table 1.1: Various ionic substitutions to apatites with a chemical formula of $X_{10}(YO_4)_6Z_2$.

$\mathbf{X^{2+}}$	$\mathbf{YO_4^{3-}}$	$\mathbf{Z^-}$
Ca^{2+}, Ba^{2+}, Sr^{2+}, Pb^{2+}, Cd^{2+}, Mg^{2+}	PO_4^{3-}, AsO_4^{3-}, VO_4^{3-}, SiO_4^{4-}, CO_3^{2-}	F^-, OH^-, Cl^-

The structure of apatite is also permissive in case of coupled ionic substitutions, as seen in some minerals like pyromorphite ($Pb_5(PO_4)_3Cl$), vanadinite ($Pb_5(VO_4)_3Cl$) and mimetite ($Pb_5(AsO_4)_3Cl$). Normally, the ionic substitutions happen in between ions with same negative or positive charge. Although, it has been observed that in some cases, these substitutions happen between ions with different charges. In this case, unequal charges and the vacancies in the structure of the apatite compensate for each other. The mentioned vacancies cause non-stoichiometry in the structure of the molecule which results in complicated crystal chemistry [11].

The basic apatite structure was almost simultaneously published by Náray-Szabó and Mehmel in 1930. Its structure is a hexagonal shape with approximate lattice parameters a = 9.37Å and c = 6.88Å and it belongs to the $P6_3/m$ space group. There are two Ca atoms which are christalographically different and three O atoms. By overseeing the distinction between O atoms, the unit cell is composed of $Ca(1)_4$ $Ca(2)_6$ $(PO_4)_6$ F_2.

1.3 Bones

Bone, or osseous tissue, is the main component that shapes the endoskeleton of vertebrates. It is a natural composite, both organic and inorganic, that is consisted of collagen fibrils which contains packed, well-organized, rod shape materials. Despite the fact that it is fixed, bone has many fundamental physiological functions [12]. It has both mechanical and metabolic functions which are classified into six different categories. They provide structural support for different parts and organs of the body, help store many important minerals and lipids for the body, reproduce red and white blood cells, protect many different organs like heart or lungs and function as a lever in many cases to change the value or the direction of the forces that muscles produce [13]. Bone tissue is a type of dense connective tissue. It has six different types based on its shape which are Sutural, irregular, short, long, flat and sesamoid count for a total of 206 bones in an adult human body.

1.3.1 Structure of the bone

Bone has a mixed composition of mineral or inorganic, organic and living content [14]. The mineral or inorganic part of the bone stands for two-third of overall composition of the bone which is shaped from impure crystals of natural calcium phosphate in the form of HA [13,15]. These crystals have a high threshold for compression forces, but are not resistant against other types of forces like twisting, bending or sudden impacts. The inorganic part of the bone is responsible for 75% of bones weight and 50% of its volume [13,14]. The composition of HA found in bone is not pure because the small crystals of apatite consist of impurities like magnesium, potassium, strontium, sodium, carbonate, fluoride or chloride [16]. The organic part of the bone stands for one-third of the bones composition. It is composed of 90% type 1 collagen fibers and 10% other proteins [14]. The collagen constituent of the bone is an extremely strong substance if against tensional forces. Because of its flexibility, it can handle twisting and bending forces very well [13]. On the other hand, bones structure can be explained on a hierarchical structural basis as well. The classification is based on the dimension of the structure, such as macrostructure which is consisted of compact and trabecular bone; microstructure which is consisted of Haversian systems and Trabeculae; sub microstructure which is consisted of Lamellae and Haversian canals; nanostructure which is consisted of collagen fiber and sub nanostructure which consists of collagen fibrils and collagen molecules [17]. Figure 1.1 illustrates the hierarchical structure of the human bone. In terms of mechanical properties, bones can be separated into two groups, cortical and trabecular bone. On the other hand, if bone is studied in terms of age and stage of development, it can be classified into two groups of woven and lamellar bone (Figure 1.1) [18].

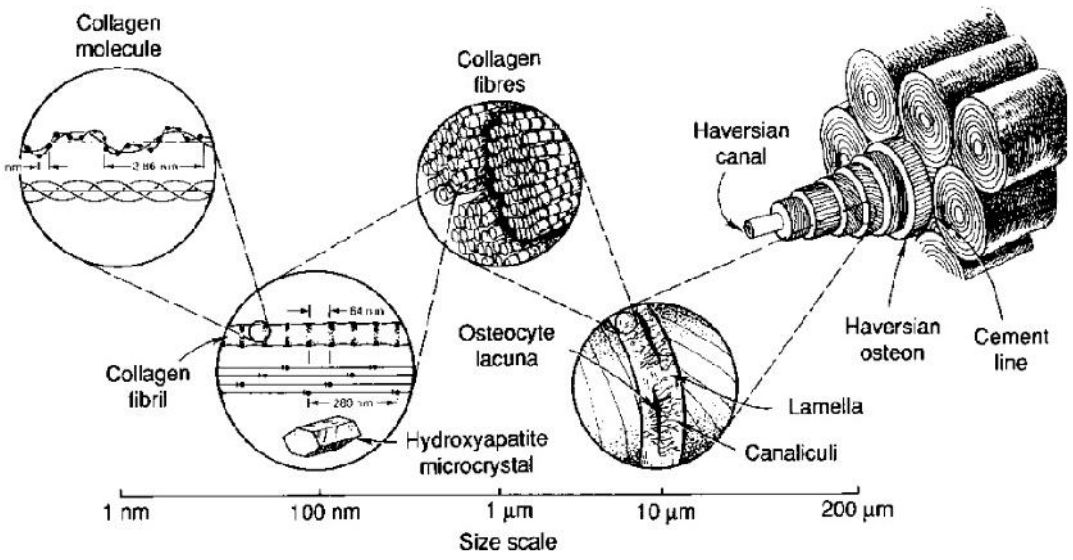

Figure 1.1: Hierarchical structure in human bone [19].

1.3.2 Compact (cortical) bone

Cancellous and cortical bones are different on many aspects including blood supply, developing stages, function, rapidity of turnover time, architecture, proximity to bone marrow and age dependent transitions [20]. The hard exterior layer of the bone is known as the compact bone because of very small and microscopic channels it has. It is very dense and has a porosity rate of 5 to 30% and protects and supports skeletal functions [20]. It is responsible for 80% of the mass of an adult human bone. [20].

1.3.3 Trabecular (cancellous or spongy) bone

The interior part of the bone is consisted of another type of the bone known as the trabecular bone which is a very porous structure based on a network of plate shaped or rod shaped elements named trabecular allowing space for bone marrow and blood vessels [20]. It accounts for the other 20% of the bones mass but its surface area is almost ten times higher than that of compact bone. Its porosity rate is 75–95% [21].

1.3.4 Mechanical properties of bone

There are different factors which influence the mechanical properties of bone. Some of them can be mentioned as porosity, density (apparent and mineral), elasticity and anisotropy.

1.3.4.1 Density

Density of the cortical bone is in a relation with its mineralization and porosity. It has been observed that cortical bone shows no difference between apparent density and mineral density values because of its structural pattern. It has been shown that the average apparent density of the cortical bone is approximately 1.9 g/cm^3. This type of bone is at its thickest and strongest where stress is applied the most because all of the osteons in its structure align with the direction of the applied stress [22]. The values for trabecular bones apparent density has been confirmed to vary between 0.14 and 1.10 g/cm^3 [22].

1.3.4.2 Porosity

Porosity or void fraction is explained as the amount of void spaces existing within any material, obtained by calculating the ratio of the void volume to the total volume. The effect of the porosity on mechanical properties of the bone is an inverse effect as the higher the porosity, the weaker the mechanical properties of the bone will be [21,23,24]. The interaction between mechanical properties of bone and its porosity follows the Equation 1.1 [24].

$$E=33.9(1-\rho)^{10.99} \qquad (1.1)$$

Where E stands for elastic modulus, ρ stands for relative density and (1-ρ) shows the bone volume fraction.

1.3.4.3 Elasticity

The cortical bone is considered to have an orthotropic or transversely isotropic structure meaning that it has diverse properties along the direction of its axis. Three different direction was recognized in a material which is considered to be transversely isotropic, being longitudinal, radial and circumferential corresponding to the bone's long axis [25]. It was observed that the length of the bone is 1.6 to 2.4 times more rigid than that of its width [22].

1.3.4.4 Anisotropy

One of the most important factors that effects the mechanical properties of bone is the direction in which loading takes place [24,26]. The utmost elastic modulus measured for cortical bone is in the longitudinal direction and the lowest value, as expected, is observed in loadings in the transverse direction. The modulus of elasticity varies for the specimens taken at any other angle between 0º and 90º [23,27]. Figure 1.2 illustrates the mentioned directions and the corresponding stress-strain diagram for different specimens. Cancellous bone also shows anisotropic and inhomogenous characteristic in its morphology [28,29]. As a result, a diverse range of values have been obtained for its elastic modulus which varies from 1 to 20 GPa [14].

1.3.5 Composition of Bone

1.3.5.1 Organic Component of the Bone

The structure of the bone is composed of a composite of different inorganic and organic substances with different types of cells embedded in its texture. These cells are of four different types which can be categorized into two different groups [17]. There are osteoblasts, osteocytes, osteoclasts and bone lining cells two of which are engaged in the resorption process and other two play a role in the formation of the

bone [17,21,22]. These cells account for a very low percentage of bones composition but are vital for assembly and maintenance of the matrix of the bone.

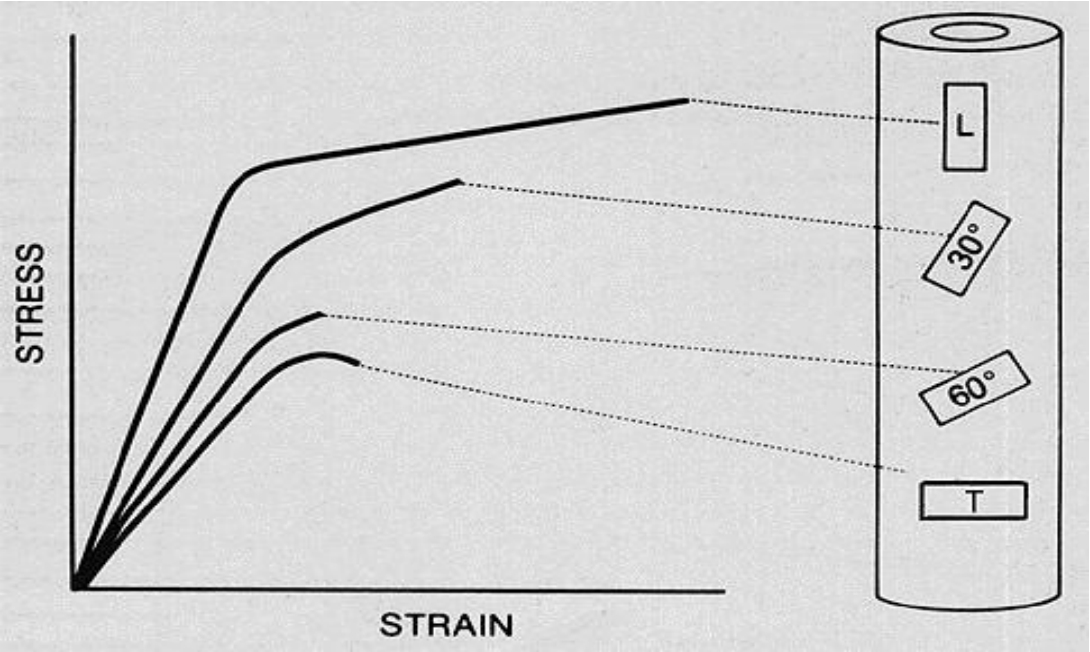

Figure 1.2: The anisotropic characteristic of the specimens taken from cortical bone. The direction of the applied loads are Longitudinal (L), tilted 30 with respect to the bone axis, tilted 60 with respect to the bone axis, and transverse (T), which greatly effects the ultimate strength and stiffness [30].

Osteoblast, are the cells responsible for production of the bone matrix, also known as osteoid. They are the main cause for sedimentation of the calcium salt compounds during calcification process by substitution of water with minerals. As a result they are responsible for shifting of the osteoid to the bone [14,21,22]. They are differentiated from osteoprogenitor cells [22].

Most common type of the cells present in the bone structure is osteocyte. They are differentiated from osteoprogenitor cells entrapped inside mineralized matrix of bone and have two important functions. First, they are responsible for bone's repair by changing into less specialized cell types like osteoblasts and help with the synthesis

of new bone. Second, they have to control the matrix of the bone for its protein and mineral content level, and renew it [14,22].

They are also the cause for osteolysis process which is the process of decomposition of the bone matrix. The equilibrium of the osteoclasts and osteoblasts is of crucial importance for bone's health because of their opposing nature [14,22].

Bone lining cells are the osteoblasts that line the bone. They are similar to osteocytes and they function as a cloak for all surfaces of the bone structure, including the blood channels. As a result they form a kind of thin cell sheet which maintains the movement of ions from body to bone and vice versa [21,22].

The organic part of the bone, as discussed before, consists of 90% collagen type 1 and 10% non-collagenous proteins including mainly glycoproteins and glycosaminoglycans (GAG). These glycoproteins play an important part in launching and regulating reconstruction and mineralization processes and they, bind minerals and collagen together [31]. As for the inorganic part, it has been shown that its structure is mostly made of amorphous HA with the chemical formula $Ca_{10}(PO_4)_6(OH)_2$. The mineral part of the bone is also considered to be either calcium or hydroxide deficient apatite and has a small crystalline size of about 20×40×200 Å. Because of its size these crystals are among the cations and anions that can be used for substitution in HA structure. Some of the cations and anions that can substitute the mineral content of the bone can be mentioned as Mg^{2+}, Sr^{2+}, Fe^{2+}, Pb^{2+}, Na^{+}, K^{+} and CO_3^{2-}, F^{-}, HPO_4^{2-} and $H_2PO_4^{-}$ respectively [31,32]. Table 1.2 illustrates the chemical fractions of mineral part of a healthy adult bone ash in wt%.

1.3.5.2 Inorganic Component of Bone

There exist various ions that can be integrated into the structure of mineral part of the bone which is mainly consisted of HA. It was reported that the integration of these ions, which exist in meager amounts, influences the mechanical properties of the bone structure [34, 35]. Some examples of these ions are Al^{3+}, Zr^{4+}, Sr^{2+}, B^{3+}, Cd^{2+}, Mg^{2+} and Si^{2+}.

Table 1.2: Chemical fractions of a healthy adult bone ash [32,33].

Ions	Amount in wt%
Calcium	32.6-39.5
Phosphorus	13.1-18
Carbonate	3.2-13
Sodium	0.26-0.82
Magnesium	0.32-0.78
Choloride	0.13
Citrate	0.04-2.67
Pyrophosphate	0.07
Potassium	0.03
Fluoride	0.020-0.207

It was observed that magnesium (Mg) ion with a +2 electrical charge constitutes 0.5-1% of the bone ash. Almost 66% of the Mg present in the skeletal system is integrated into the structure of HA and can be dissolved in the resorption process. The lack of Mg^{2+} ions has a negative effect on the metabolism of the skeletal system and interrupts the natural growing process of bone, reduces the activities of osteoclast and osteoblast cells and makes the bone more brittle [36]. It was reported that the amount of Mg present in bone tissue can vary by aging. Its concentration is high in cartilage and bone along the first levels of osteogenesis but starts to decrease as the bone tissue matures [37].

Zirconium (Zr) is another material which undergoes ionic exchange with HA, the main inorganic constituent of the bone structure. It was reported that ZrO^{2+} ions are exchanged with Ca^{2+} ions from HA. The radius of ZrO^{2+} ion has been reported to be 0.21 nm, whereas that of calcium ion is about 0.1 nm. As a result, an increase in the unit cell of HA is observed as the ZrO^{2+} ions substitute those of the Ca^{2+} [38]. It was shown that the substitution of the Zr^{4+} ions with those of phosphorous ions in Ha structure is highly unlikely because of the difference in their size. The radius of the P^{5+} ion and Zr^{4+}ion has been reported as 0.38 and 0.72 nm, respectively [38].

Another material which is observed in bone structure is Silicon (Si) with the atomic number 14. It was reported that Si has the highest concentration in the connective tissues because it is an integral component of GAGs and their protein complexes, which play an important role in tissue structure. It was shown that nutritive silicon addition will not enhance growth or skeletal system development. It was also reported that despite the fact that silicon escalates mineralization the lack of it will cause bones to develop abnormal shapes [39].

Boron (B) is a crucial material for the life of many plants, but it is not proved that it has the same importance for the mammals. It was reported that low levels of B in a diet will intensify the effect of vitamin D deficiency in bone, thus the role of B in bone metabolism [39]. Another study was conducted on postmenopausal women showing that an increase in the intake of B resulted in increase of estradiol and testosterone concentration and so it was shown that B has a positive effect on postmenopausal osteoporosis. Another research was conducted analyzing a boost of B intake, in the form of boric acid, on rats from 0 to 9000 ppm for 9 weeks. It was reported that after the experiment was ended, the value for urine and serum dropped to normal but bone reserved its high B levels for 32 weeks after the cessation of the diet. The only change observed was 5-10% more resistant to crush forces [39].

Aluminum (Al) is another metallic ion that effects the process of mineralization in bone. It was reported that the calcification and mineralization of the bone was influenced by Al concentration however separating the physiochemical effects from biological ones was not possible. Al^{3+} ions are another group of ions competing with calcium, and suppressing the formation of HA in mineralization process [40]. It was mentioned that regarding the toxicity of the Al, the required amount of Al concentration for the calcification process to be interfered was higher than that was observed. It was reported that the best indicator for the toxicity of the Al was the surface stainable amount of it, which effects the calcification and mineralization process negatively when above 30%. Al toxicity happens to patients with chronic renal failure because of Al accumulation. It was shown that the preferred medicine for tearing these group of patients are chelators. Treatment with desferrioxamine and

removal of exogenous Al sources in the body is conducted carefully in order to prevent other side effects like infection [41].

Cadmium (Cd) is an important metallic ion that can be integrated into the structure of the bone, but it is both toxic and carcinogen, reducing its chance of being used in medical applications. It was reported that Cd effects three organs the most, which are kidneys, skeleton and the respiratory system, particularly involved in acute poisoning. It was reported that constant exposure to Cd worsens the uncoupling effect between the formation of the bone and its resorption in rats with ovariectomy syndrome, validating the decreased mechanical strength effect on bone in case of constant exposure to Cd. It was also reported that Cd causes diminished calcium absorption and increased calcium loss from the bone [42,43]. It was reported that Cd has a double effect on the bone, one being direct contact with bone cells, causing cessation of the mineralization and inhibiting the procollagen C-proteinases, thus suppressing self-assembly of the collagen in the cellular matrix which results in a notable decrease in collagen production [39].

Strontium (Sr) goes through the same metabolic channels as calcium. It substitutes calcium ceasing mineralization and formation of the bone [39]. It was reported that normal progression of the osteoid towards bone was restricted with an increase in the Sr^{2+} amounts. Strontium was also used in radiotherapy of patients of bone metastases. This method was commonly used for reducing the pain in patients with prostatic cancer and has also been used for patients with breast cancer [39]. Strontium is believed to have positive effects on bone like boosting the reproduction of preosteoblasting cells. Strontium ranelate, a kind of Sr salt, has been reported to decrease the rate of resorption in bone, giving way to more bone formation and thus increasing the strength of the bone [44].

Lanthanum (La) with an atomic weight of 138.09 is a rare-earth element which has chemical associations like those of Sr, Ca and Barium (Br). Lanthanum and its applications has been investigated and become of interest because lanthanum carbonate is a possible substitution for phosphate binders of calcium base. These binders have been widely used as the main treatment for decreasing the level of

plasma phosphate in patients of hyperphosphatemia suffering from end stage renal disease (ESRD) [39,45]. It was reported that increased levels of calcium intake causes cardiovascular calcification, hyper calcemia and a higher probability of cardiovascular disease. Lanthanum sedimentation happens first at the liver as it enters the circulation, then is becomes endocytosed in the cytosome of liver cells and then transferred to the bile. What remains of lanthanum is deposited in bone or excreted to urine. Lanthanum is deposited in bone, both in the surface and in the inner part and the rate of its progression towards the inner side is very slower than that of calcium's. With the continuous intake of lanthanum, bone becomes the main site for lanthanum deposition in the body. It was reported that as the intake stopped, bone lost its lanthanum content with a rate of 13% per annum measured in a dialysis population. This rate of loss of lanthanum, which is very much higher than what was estimated for healthy adults, takes place because of the ionic transaction happening at the surface of the bone and because of the bone resorption process controlled by osteoclasts, which in turn, will result in bone turnover. It was invesitegated that lanthanum has a tendency to compile and concentrate on the surface of the bone which gives its ions a change to be exchanged with compartments of body's fluid [39,45].

1.4 Hydroxyapatite

HA has a similar chemical structure to the bone's inorganic part. It's chemical formula is $Ca_{10}(PO_4)_6(OH)_2$ [46,47]. It is extensively used as a synthetic biomaterial and as a bulk material for non-load bearing implants, because of its fine biocompatibility, non-porous bioactive surface, density, and the ability to establish chemical bonding with the bone which is known as bioactive fixation [48]. It has a 1.67 Ca/P ratio in stoichiometric form. It is most favorable, since its pH is the most stable in calcium phosphates with pH above 4.2-8.0 range which has the benefit of lowering the risk of corrosion. Previous studies have reported the use of HA as implants as a coating applied on the metal to improve its osteointegration. These kinds of HA coated metallic implants are mostly used in dental implants, hip joints

and knee joints [48]. HA improves the ability of bone tissue to establish chemical bonds with the surface of the implants and hastens the rate of bone growth, increasing its application in biomedical implants and industry. However, having insufficient mechanical properties such as low hardness, fracture toughness and strength, restricts it use for the load bearing areas of the body [49].

1.4.1 Structure of HA

Stoichiometric HA has a general molecular formula of $Ca_{10}(PO_4)_6(OH)_2$, in which the ratio for Ca/P is equal to 1.67. HA has two crystalline structures, hexagonal and monoclinic. The theoretical structure of HA is monoclinic in which unit cell parameters are a=9.42148 Å, b=18.842, c=6.88147 Å, γ=120° and space group $P2_1/b$, but it is very hard to produce HA with the monoclinic structure [50]. On the other side it has been reported that HA can possess a hexagonal structure with parameters a = b = 9.432 Å and c = 6.881 Å and the space group will become $P6_3/m$ [51]. The hexagonal structure is composed of six calcium atoms surrounding six tetrahedral phosphate groups and another attaching site for four calcium atoms being the center of an equilateral triangle positioning on the screw axis. The structure includes two OH^- molecules pointing out in the opposite direction positioned in the columns on the axis. It is the steric conflict between these two neighboring OH^- molecules that provides the possibility of ionic substitution for HA with different ions like F^- and Cl^-. The only difference between the monoclinic and hexagonal structure is in the orientation of the OH^- molecules which in the monoclinic structure happen to point to the same direction, giving the monoclinic HA improved stability and order and thus, being the favorable stoichiometric structure [51,52].

The structure is composed of six tetrahedral phosphate group that are surrounded with six Ca atoms. Figure 1.3 illustrates the atomic structure of HA with a $P6_3/m$ space group.

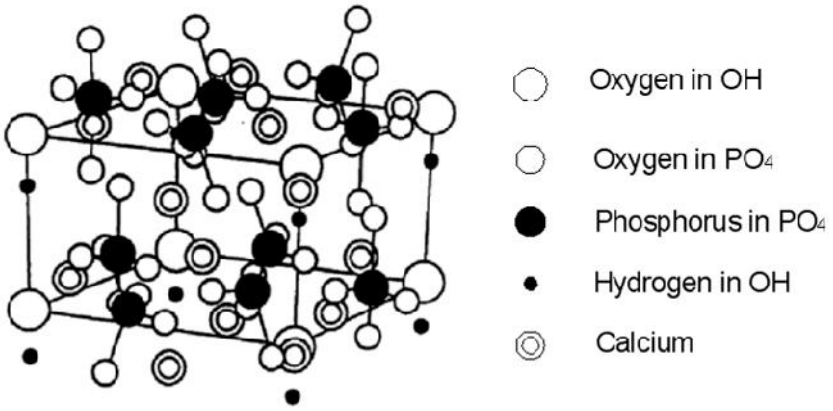

Figure 1.3: Hexagonal structure for HA with a P63/m space group [52].

1.4.2 Synthesis methods for HA

There are different ways to synthesize HA which includ precipitation method, solid state method, wet chemical method, sol-gel method, hydrolysis method, emulsion and micro emulsion method and some chemical methods. Some of the most common ones are explained as follows.

1.4.2.1 Solid State Method

In order to synthesize HA using this method, some chemical reactions of acidic nature must be conducted. As the first step the required inorganic medium is prepared using either water or acetone. After that the mixture is milled for different periods of time depending on the experiment using ZrO_2 balls and then dried in a convection oven and heat treated [53,54]. The process of milling with ZrO_2 balls is of dire importance because during this period the size of products powder particles become smaller without formation of a new phase and it also prevents contamination [54]. It was also reported that the heat treatment procedure plays an important role in this method since the product undergoes phase transitions in this procedure which was confirmed by XRD [53]. It was observed that the HA produced via this method demonstrates favorable biocompatibility and enhanced

mechanical properties. Products and materials synthesized via this method possess better hardness levels than that of the natural bone, although their density does not vary from one another [54].

1.4.2.2 Sol-gel

This method is one of the wet chemical methods that can be used for synthesizing HA, which unlike some methods does not need to be stirred in a high temperature and also does not need a high pH value. It was reported that HA obtained via this method undergoes a process in which phosphorous and calcium are mixed at the molecular level, thus presenting very good chemical homogeneity [55]. Figure 1.4 displays the hierarchical steps for synthesizing HA via sol-gel method. Because of the reactive characteristic of the sol-gel powders, the temperature of the process is reduced and thus, the size of the crystalline nanoparticles of the resulting product decreases, making this method a more favorable one [56]. It was observed that as the sintering period and temperature increases, the degree of crystallinity of the synthesized powder increases [55].

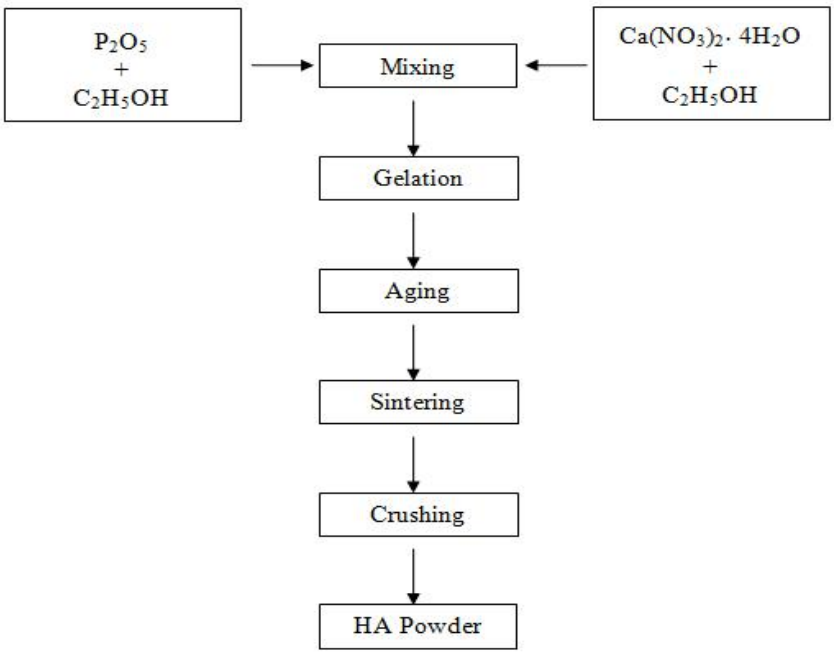

Figure 1.4: Stages of sol gel method [55].

1.4.2.3 Precipitation

HA has been very useful in biomedical applications because of its unique resemblance to bone and mechanical and biological properties. As a result, some different methods had evolved to synthesize it that can be clustered in two groups which regarding the undergoing process are named wet synthesis and dry synthesis methods. The advantage of such methods are that they have water as their byproduct and that they have a very low chance of contamination during the process [54]. One of the wet synthesizing methods is the precipitation method. In order to produce HA via this method calcium nitrate and ammonium phosphate are used as starting materials. Since controlling the pH of the solution is important, ammonia is used in the process of preparing the mixture. Using calcium nitrate and ammonium phosphate, two different solutions are prepared and sintered at room temperature (RT) [57]. After that di- ammonium hydrogen phosphate solution is poured drop wise into calcium nitrate mixture and followed by an addition of ammonium for the purpose of adjusting pH [57]. To achieve a product cake, and using some filtering papers, the HA precipitate is removed from the mixture, then underwent drying, calcification and sintering processes. It was observed that the product grain size of this synthesize method is strongly affected by the pH of the solution and the temperature of sintering [57]. It was also reported that because of the fine-grained structure of the HA obtained by this method, it has a better biocompatibility and is more favorable by the host tissue [58].

1.4.2.4 Hydrolysis

This method is based on synthesizing HA via hydrolysis of dicalcium phosphate dehydrate (DCPD), a precursor of the HA, which accumulates along the c-axis following this chemical reaction:

$$10CaHPO_4 \bullet 2H_2O \rightarrow Ca_{10}(PO_4)_6(OH)_2 + 18H_2O + 12H^+ + 4PO_4^{3-} \quad (1.3)$$

DCPD dissolves and converts to HA in a rapid solid-solid transition taking place at

a high liquid-to-solid ratio. Calcium deficient HA (d-HA) is formed as a result of using DCPD as starting material. The resulting d-HA material, having a Ca/P ratio of about 1.33-1.67 and the structure of a crystal apatite, decomposes to form stoichiometric HA and β-TCP.

Equation 1.4 shows the two phases of the reaction. The first step changes the structure of the DCPD to that of the crystal apatite with a lower Ca/P ratio, and then the second step corrects the ratio by making an adjustment to the composition of the material.

$$DCPD \rightarrow HA(Ca/P<1.67) \rightarrow HA(Ca/P=1.67) \qquad (1.4)$$

1.4.3 Mechanical properties of HA

Since HA, being a ceramic material, shows different characteristics as the duration or the temperature of the sintering process changes, its mechanical properties like tensile or compressive strength, elastic modulus, hardness, bending and other properties are expressed as a range of data [59]. Because of HA's inferior fracture toughness (<1 $MPa.m^{1/2}$) and ductility, it has a brittle nature. Also its mechanical properties is negatively affected by its decomposition to different phases of TCP [60]. Therefore improvement of its mechanical properties has attracted wide attention. As stated in the results obtained from numerous experiments, the range for bending strength has been reported to vary between 38-250 MPa, its compressive strength vary between 120-150 MPa, its tensile strength vary between 38-300 MPa and modulus of elasticity was reported to vary in the range of 35-120 GPa for HA undergoing sintering at 1000-1100ºC, which is stronger than that of the spongy bone (almost 17.7 GPa) and that of compact bone (almost 22.5 GPa) [59,61,62]. It was reported that porosity and impurity etc. had influenced these results as well [59]. Porosity as another aspect of HA has altered its biocompatibility and mechanical properties, as it was observed that it is in an exponential relationship with hardness and elastic modulus of the material [63,64,65]. It was reported that the porosity of the HA has an almost inverse relationship with its fracture toughness, so that as the porosity decreases, the toughness increases and also an increase in the micro porosity

of the HA structure results in a decrease in its compressive strength [66]. It was stated that depending on the temperature of the sintering process, fracture toughness of HA can be divided into three intervals of 1100-1150ºC, 1150-1250ºC and above 1250ºC, in which with the increase of the sintering temperature the fracture toughness of the samples was increased, remained constant, and decreased respectively [49]. It was also stated that elastic modulus, compressive strength, density and grain size are in a direct relationship with sintering temperature [67].

Anisotropy of the HA crystals was studied and the results showed that hardness (7.06 GPa) and Young's modulus (150.4 GPa) have higher values in the crystallographic direction of (0001) than hardness (6.41 GPa) and Young's modulus (143.6 GPa) values in the (1010) direction [68].

Another study reported the data for measuring the bending strength in air and in water for a single crystal of the structure of the HA and reported the results to be 500 MPa and 454 MPa, respectively, which is approximately 2.4 times the bending strength for dense HA (113-196 MPa) [69].

1.4.4 Biological properties of HA

HA is considered to be a very biocompatible and bioactive material because of its structural resemblance with mineral part of the bone, which accelerates bone growth rate while integrated with the material and also because of its ability to make chemical bonds with the bone tissue [70,71]. Likewise, HA has a stable nature in watery environment with a pH range of 4.2-8.0, which reduces the corrosion probability for implant. It was also reported that a layer of HA is applied on the surface of the implant metal to improve osteointegration. Porosity is another important property of the bone which highly affects the biocompatibility of the HA and increases vascularization and bone formation. On the other hand, surface topography greatly affects proliferation of osteoblasts and cell adhesion to the surface [71]. It was observed that in HA samples with pore diameters of 400 μm, cell penetration and movement increased. It was reported that cells spread and progenitor

cell proliferated within two weeks, and after one month the differentiated cells shape their own setting, leaving some spaces empty for the vascularization and mineral transfer, and filling the rest [71]. In an in vitro study the effect of different pore sizes was investigated. The results showed that pore sizes within the range of 400-1600 μm enhanced bone regeneration and induced attachment of bone morphogenic protein at the surface which is a sign of HA's osteoconductive property [71]. Another characteristic of the biocompatible HA is its crystallinity. It was reported that HA with crystal structure enhanced the new bone formation and tissue growth. It was stated that HA with nano crystal structure possessed more surface area than that of micro structure or the control group [71].

1.5 Zirconia

Zirconium dioxide, is a white crystalline oxide of zirconium. ZrO_2 has three different structures including monoclinic, tetragonal and cubic, from which monoclinic is the most occurring from [72,73]. There has been a fast growing interest in the biomedical applications of ceramics in past years. HA, being a bioactive ceramic, possesses favorable biocompatibility and enhanced bone bonding ability [74]. However, the mechanical properties of the sintered HA, do not meet the requirements of an implant. The compressive strength of the cancellous bone and cortical bone is 12 and 200 MPa respectively, while previous studies have shown the compressive strength of the synthesized porous blocks of pure HA to be 0.3 MPa [75]. A bio ceramic composite formed by HA and ZrO_2 can be an alternative. ZrO_2 does not have a good tissue or cellular affinity, however, it is a good choice because of its strong mechanical properties, good wear and corrosion resistance and biocompatibility.

1.5.1 Mechanical properties of ZrO_2

At RT, pure ZrO_2 takes the monoclinic structure and stays stable up to 1170ºC. As the temperature increases, ZrO_2 undergoes a phase transition to tetragonal and after

that, at 2370ºC, to cubic phase. It was observed that a phase transition takes place during the cooling process which is assumed to happen as a result of an approximately 3-4% volume expansion, which in turn, causes cracks in the structure of the ZrO_2 that breaks to pieces after sintering [73]. Moreover, it has been shown that a stress-induced phase transformation of ZrO_2 from tetragonal to monoclinic phase has resulted in the increase of its strength and fracture toughness. It was reported that precipitates of tetragonal structure which were well diffused into the cubic network underwent a transition to monoclinic phase as the constriction forced upon them by the network was relieved by means of a crack. As a result, the stress-induced force created because of the expansion resulted by the phase transition opposes the stress-induced force which causes the development of the crack throughout the material (Figure 1.5). Since the energy force driving the development of the crack is dispersed between the stress caused by the expansion and the phase transition, the toughness of the samples is improved [73].

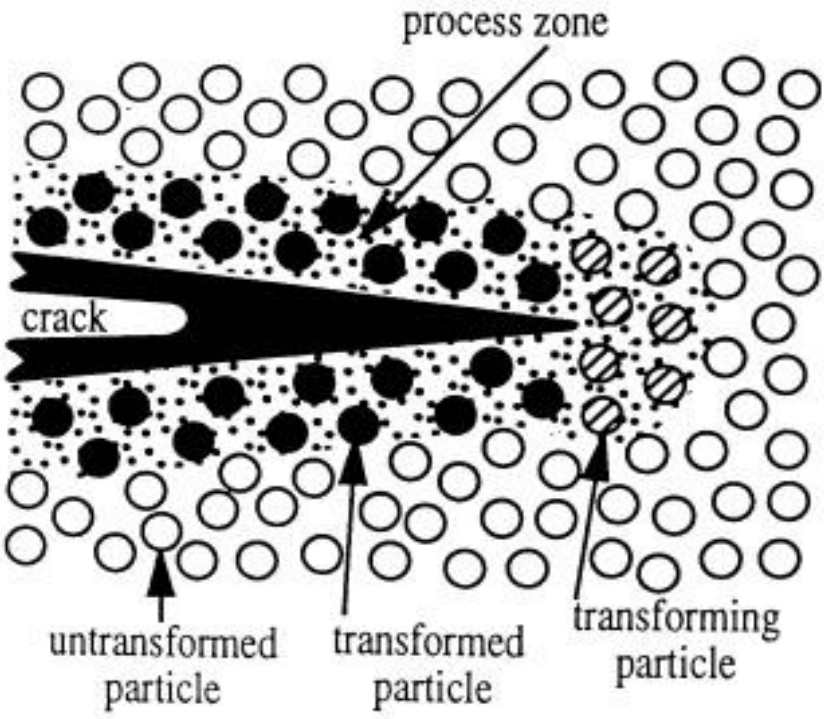

Figure 1.5: Illustration of the toughening process as a result of the stress-driven transformation [73].

In HA-ZrO_2 composites, HA can decompose at lower temperatures, which leads to formation of second phases, and ZrO_2 undergoes a transition from tetragonal to cubic structure which weakens their mechanical properties [76]. It was observed that in sintering processes with temperatures higher than 1000ºC, the calcium from HA dispersed into the structure of ZrO_2 causing HA to decompose to TCP. HA follows Equation 1.5 in decomposition to second phases [76].

$$Ca_{10}(PO_4)_6(OH)_2 \leftrightarrow 3Ca_3(PO_4)_2+CaO+H_2O \quad (1.5)$$

CaO produced in this reaction then engages in another chemical reaction with ZrO_2 to form $CaZrO_3$ through Equation 1.6.

$$CaO+ZrO_2 \leftrightarrow CaZrO_3 \quad (1.6)$$

It was reported that this reaction happens at temperatures above 1200ºC and was confirmed by XRD analysis [76]. Since the fluorite structure of the tetragonal ZrO_2 is a distorted one, oxides such as CaO, Y_2O_3 and MgO exhibit high rate of solid solubility in it. While CaO dissolves in tetragonal ZrO_2, it undergoes a phase transition and turns to cubic ZrO_2. Calcium oxide then reacts with tetragonal ZrO_2 to form cubic ZrO_2 (Equation 1.7) which in turn, forces Equation 1.5 to move forward and decompose HA to produce CaO [76].

$$CaO+t\text{-}ZrO_2 \leftrightarrow c\text{-}ZrO_2 \quad (1.7)$$

Figure 1.6 illustrates the phase transition from monoclinic phase to tetragonal phase in temperatures higher that 1200ºC.

Compressive strength of the ZrO_2-HA composites was enhanced noticeably as the amount of ZrO_2 increased in the content of the composites [80]. It was reported that the compressive strength of these scaffolds was increased from 0.3±0.01 to 13.8±0.94 MPa with the increase of ZrO_2 content in the composite from 0 to 100% [75].

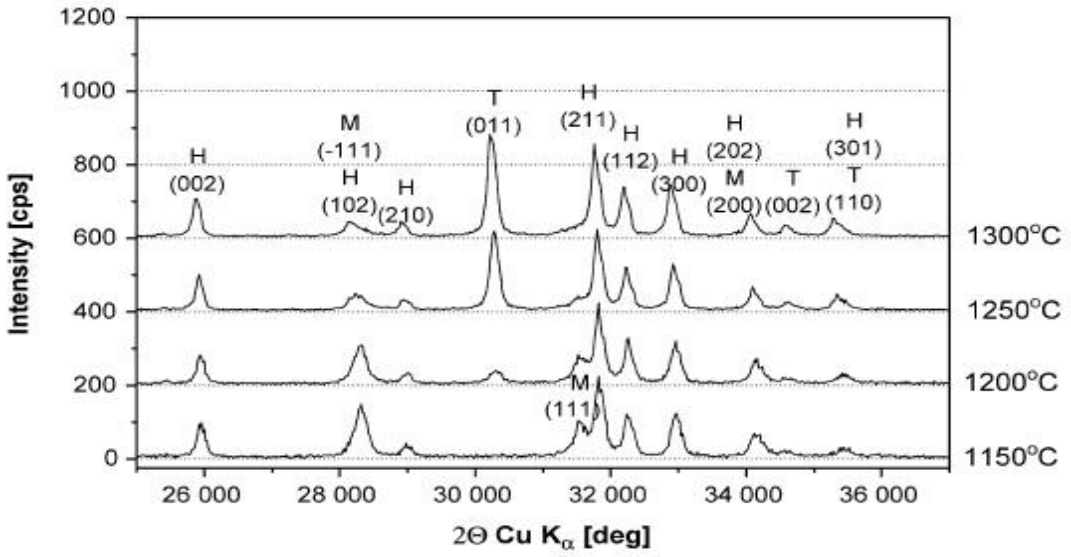

Figure 1.6: Phase transition from monoclinic ZrO_2 to tetragonal ZrO_2 [77].

It was reported that Y_2O_3 stabilized ZrO_2 has the best possible mechanical properties amongst other compositions and thus is the main kind used in medical implants. It has shown a resistance to traction as high as 900-1200 MPa. ZrO_2 was also studied for its cyclical stress tolerance. It was reported that with a periodic force of 28 kN, some 50 billion cycles are required to break the samples [72]. The life time of some metal free cores for fixed partial dentures (FPD) was studied. It was reported that ZrO_2 with Al_2O_3 possesses the highest initial and most pleasing long term strength rate [72]. In another study, the mechanical resistance of ZrO_2 FPD's was investigated on the restoration of a single tooth and the resulting fracture load was reported to be over 2000 N [78]. The ageing of ZrO_2 was investigated in another study. It was expressed that ageing has damaging effects on mechanical properties of ZrO_2 and that mechanical stresses and exposure in wet mediums demolishes and hastens this process. However, it was investigated in an in vitro study that the mechanical properties of ZrO_2 decreases with ageing, the decreased values are still in the clinical acceptable range [79,80].

Surface modification is another property that can enhance mechanical properties of ZrO_2. The removal torque and osteointegeration of ZrO_2 with a modified surface, ZrO_2 and titanium oxide implants were compared which were removed from femur

and tibia of rabbits. It was reported that although they seemed to have the same amount of integration, the removal torque for pure ZrO_2 was lower than that of the other two, implying that surface modification improves the stability of the implant [81].

1.5.2 Biocompatibility of ZrO_2

The optimal substitute material that can be used in an implant for bone or skeletal system defects should have different conditions including mechanical porosity, biocompatibility and mechanical stability. It is crucial for the material to be biocompatible, meaning that the material should not illustrate any kind of cytotoxic or immunogenic behavior or cause any unsolvable inflammatory response. The attachment of the osteoblast cells to sample composites of HA and ZrO_2 with different ratios was studied using Scanning electron microscopy and the results showed that attachment is at its best in compositions with 20% weight of ZrO_2. A previous study illustrated that ZrO_2 has a low attachment tendency for proteins and claimed that low attachment tendency in samples with higher ZrO_2 ratio has the same reason. Improved osteoblast adhesion was measured on HA-partially stabilized ZrO_2 composites at 900C and with 10wt% PSZ and 90wt% HA composites [75]. The first evaluation on biocompatibility of ZrO_2 was conducted in 1969 and it was reported that no negative effects was cited during the procedure in which ZrO_2 was put inside a monkey's femur. An in vitro study confirmed that ZrO_2 is not a cytotoxic examining the behavior of the cells [72]. Two different groups evaluated mutagenicity of the ZrO_2 and both reported that ZrO_2 is incapable of causing mutations in cells genome.

Another study investigated the rate of bacteria growth on a ZrO_2 surface and reported that ZrO_2 surface used was covered by bacteria by a 12.1% whereas titanium surfaces was covered by a 19.3% coverage proving bacteria adhesion on ZrO_2 surface to be in an acceptable range. These results were confirmed by an in vivo study in which the total number of bacteria was studied, showing that tetragonal ZrO_2 polycrystal (TZP) had a lower number in comparison to titanium [82]. It was

reported that zirconium oxide restorations are reliable for clinical use on the basis of a study examining the result of ZrO_2 ceramics inserted in 18 teeth after three years, which has just one failure [83].

1.6 Boron

Boron (B) is obtainable form over 200 different natural minerals like colemanite, tincal, ulexite and kernite. Boron and its derivatives are widely used in industry to manufacture many diverse products including textile, borosilicate glass, enmals, disinfectants and drugs. Boron enters our body mainly through our drinking water and diet. The standard mean for boron levels in drinking water is between 0.1 and 0.3 mg boron/L. Boron compounds intake happens via the respiratory or gastrointestinal systems in human body up to 90%, but it also exerts through the urinal track in several days [84].

1.6.1 Mechanical Properties

Addition of B as a boron nitrate compound (BN) to the HA has significantly improved its mechanical properties. Surface morphology of the samples of pure HA and HA-boron nitrate composites were investigated and it was reported that theoretical density of the HA-BN composite (97.0% ± 0.3%) was higher than that of pure HA (92.2% ± 1.1%) [85]. Thermal conductivity of the BN composites was compared with that of HA and it was confirmed that HA-BN composites have higher thermal conductivities (200-300 W/mK) in comparison with HA (1.25 W/mK). It was showed that BN effects the grain size in composites of HA. As reported, HA-BN composite possesses a grain size of 0.17 ± 0.1 μm, where pure HA has a grain size of 0.61 ±0.16 μm which is almost three times bigger than that of HA-BN's [85]. The depth of indentation was studied in HA-BN composites. The results displayed higher rates for indentation depth in pure HA samples which in turns confirms lower hardness (6 ± 1 GPa in comparison with 12 ± 2 GPa) which is a 100% raise in hardness for HA-BN composites. Elastic modulus of the HA and HA-BN samples

was investigated and results were reported as 93 ± 9 GPa for HA-BN composites where HA samples showed an elastic modulus of 205 ± 15 GPa which is an increase of 120% [85].

1.6.2 Biocompatibility

Biocompatibility and bioactivity of BN compound were studied to confirm that there is no cytotoxicity threatening the macrophages and osteoblasts, which are the two most important cell lines in orthopedic applications and it was reported that they are non-cytotoxic. Composites of BN were also found to be not toxic to human neuroblastoma cell line and human embryonic kidney cells. Proliferation and growth rates of osteoblast cells on HA and HA-BN sample surfaces were studied after a period of 3 days. It was stated that both show osteoblast proliferation, although the rate of growth for HA-BN composite is slightly higher. The expression of genes on the surface of samples was investigated and results illustrated that BN enhances the proliferation and growth of osteoblasts [85].

1.7 Lanthanum

Rare earth elements (REE) are one of the resources that is being used extensively in different aspects of life involving medicine, industry and daily life. Lanthanum, being a member of the lanthanides family is an important material that has noticeable mechanical properties and biological compatibility with human body. It was investigated and proved that lanthanum ultimately accumulates in the body, thus urging the scientists to do vast researches assessing the effect of lanthanum on general health of the body. Lanthanum is a trivalent member of the REE family which is present in the body in trace amounts [86]. It was reported that the rate of gastrointestinal adsorption for lanthanum is less than 0.00089%. It was reported that as a result of a physicochemical affinity between strontium, uranium, aluminum and lanthanum with calcium, these mentioned materials prefer to accumulate in the bone. Since La^{3+} have a slightly larger radius than that of Ca^{2+}, it replaces Ca^{2+} in HA

which is the main constituent of the bone, consequently leading to expansion of the HA lattice. Because La^{3+} has more positive charge than Ca^{2+}, and because of its high electro positivity, it is a strong acceptor with a high tendency towards anions with oxygen in their structure. Thus, carboxyl and phosphate groups are considered the most common biological ligands which form tight complexes with lanthanum [87].

1.7.1 Mechanical Properties

In order to stop crack deflection, crack growth and interfacial debonding, lanthanum phosphate ($LaPO_4$) has been introduced into ceramic matrix composites. It was reported that $LaPO_4$ has successfully regulated the process of grain growth in alumina-$LaPO_4$ composites. It was also reported that $LaPO_4$-ZrO_2 composites are machinable and thermally stable [87]. Flexural strength (FS) of the La-incorporated and La-free apatites was studied. It was reported that the FS values measured for the La-incorporated apatite are noticeably enhanced (up to 3.2 times) in comparison with La-free HA blocks. It was also reported that embedding La into the matrix of HA enhances the microstructure of HA by further densification during sintering. It was concluded that low FS values for La-free HA blocks are originated in its larger porosity and higher degree of decomposition and absence of La in its matrix [86]. It was showed that dissolution rate for La-free apatites has a higher value than that of La-incorporated one and the difference grows bigger as the La content of La-incorporated apatites increase. Since apatite is a member of ionic crystals, its energy of crystal lattice depends heavily on ionic charge and ionic radius. In case of replacing Ca^{2+} with La^{3+} , the ionic charge is increased by 50% but the ionic radius experiences a slight change from 0.99 Å to 1.016 Å which enhances the energy of crystal lattice, thus the lower dissolution rate and higher thermal stability of the La-incorporated apatites [86].

1.7.2 Biocompatibility

Neurotoxicity of La was investigated by giving lanthanum chloride to a group of wistar rats and it was observed that La effects the functions of the brain depending on its intake dose. It was also reported that La^{3+} improves the evolution of osteoclast-like cells and in a concentration of 1.00×10^{-8} mol l^{-1}, it increases the surface area and number of resorption pits noticeably, but in concentrations higher than that, it prevents the process of bone resorption. It was also observed that La^{3+} has some favorable effects on human health including resistance and prevention of diffusion of cancer cells, treating hypophosphatemia, constraining human red blood cells Ca pump, maintaining the effects on functions of platelets via reducing lipid fluidity of the surface membrane of the human platelet [86].

1.8 Aim of the study

The goal of this study is to investigate microstructure and mechanical properties of composites of HA with ZrO_2, B_2O_3 and lanthanum oxide. HA was synthesized via precipitation method and then sintered at 1100ºC for 1 hour. Density, Energy dispersive x-ray spectroscopy, fourier transform infrared spectroscopy and X-ray diffraction tests were conducted in order to confirm establishment of bonds and phases. To study the microstructure of the samples, mercury intrusion porosimetry and scanning electron microscopy was carried out. Diametral strength and micro-hardness and drilling tests were executed to investigate to mechanical properties and machinability of the samples. For the biocompatibility analysis, in vitro test was performed using Saos-2 cell line. in order to measure the proliferation of cells PrestoBlue™ viability test was conducted on cells seeded on samples sintered at 1100ºC for 1h. Morphology of the cells on sample discs was investigated by SEM.

CHAPTER 2

MATERIALS AND METHODS

2.1 Precursor Materials

Chemical precursor materials used for synthesizing pure HA were calcium nitrate tetra hydrate ($Ca(NO_3)_2{\cdot}4H_2O$) di-ammonium hydrogen phosphate ($(NH_4)_2HPO_4$) (Merck, Germany), and ammonia. In addition to these materials ZrO_2, B_2O_3 and La_2O_3 compounds were used for composite samples. In HA- ZrO_2 composites commercially available ZrO_2 and La_2O_3 (Aldrich, Germany) were used and for HA-B composites Boric anhydrate (B_2O_3) (Sigma-Aldrich, Germany) and La_2O_3 (Aldrich, Germany) were used. For pH adjustments, ammonia solution was used (NH_4OH) (Merck, Germany).

2.2 Materials used for cell culture experiments

For culturing cells, Dulbecco's Modified Eagle Medium (DMEM) with high glucose level and fetal bovine serum (FBS) were obtained from Biochrom, Germany. PrestoBlue™ was obtained from Invitrogen, USA. Trypsin-EDTA used for cell detachment and Penicilin-streptomysin were provided by PAA Laboratories GmbH, Austria. For preparing SEM specimens, gluteraldehyde and hexamethyldisilizane and 100% ethanol (Sigma-Aldrich, Germany) were used.

2.3 Synthesis Method of Pure HA

Pure HA samples were synthesized via precipitation method and calcium nitrate tetra hydrate ($Ca(NO_3)_2{\cdot}4H_2O$) and di-ammonium hydrogen phosphate ($(NH_4)_2HPO_4$) were used as precursor materials. To achieve a theoretical Ca/P ratio of 1.67, these two powders were mixed in different amounts in distilled water and stirred for 1 h. Afterwards, ammonia solution (NH_4OH) was added to the diammonium hydrogen phosphate mixture and the resulting solution was left stirring for 10 minutes. Calcium nitrate tetra hydrate solution and some ammonia were added drop wise to the previous obtained mixture and ammonia was used to adjust the pH to be in a range of 11 to 12. The resulting solution was heated till reaching the boiling point while being stirred in order to speed up the reaction. Then the solution was stirred overnight and afterwards filtered through a fine filter paper, producing a wet cake. In order to remove the excess water and ammonia in the mixture, the wet cakes were then put in an oven overnight and dried at 200ºC. Following this stage the samples underwent sintering at 1100ºC for 1h.

2.4 Synthesis Method of HA-ZrO_2, B_2O_3 and La_2O_3 Composites

In order to synthesize the composites, commercial tetragonal zirconia (t-ZrO_2), B_2O_3 and La_2O_3 were added to the initial precursor material used for preparation of pure HA, to achieve the required composites of HA-ZrO_2-La_2O_3 and HA-B_2O_3-La_2O_3. 8 different composites were synthesized and their details are presented in Table 2.1.

In order to synthesize the composites, the powders were weighed according to the defined ratio and then mixed in pure ethanol and left for stirring for 3-5 hours to obtain the best composite structure and then dried in an oven over night to remove the excess alcohol. Then the resulting composite powder was milled and further mixed in a mortar and pestle to achieve the perfect distribution. After that the composite powders were cold pressed in tool-steel die to form pellets with an automatic hydraulic press under 10 kN force for 1 minute. The resulting pellets had a

diameter of 1 cm and about 2-3 mm thick. Finally, obtained pellets were sintered at 1100ºC for 1h.

Table 2.1: Different compositions and their wt%.

Sample ID	wt % HA	wt % t-ZrO_2	wt % B_2O_3	wt % La_2O_3
90HA10Zr	90	10	0	0
88HA10Zr2La	88	10	0	2
80HA20Zr	80	20	0	0
78HA20Zr2La	78	20	0	2
90HA10B	90	0	10	0
88HA10B2La	88	0	10	2
80HA20B	80	0	20	0
78HA20B2La	78	0	20	2

2.5 Characterization Methods

2.5.1 Structural Analysis

2.5.1.1 Density

After sintering the composite samples, their bulk densities were obtained by measuring their dry weight and calculating the volume by measuring the dimensions of the obtained pellets using the following formula:

$$\rho = m/V \qquad (2.1)$$

Theoretical density of the composites (components a, b and c) was calculated using the densities, ρ, and known weights, W, via the following formula:

$$\text{Density } (g/cm^3) = \frac{W_a + W_b + W_c}{\left(\frac{W_a}{\rho_a}\right) + \left(\frac{W_b}{\rho_b}\right) + \left(\frac{W_c}{\rho_c}\right)} \qquad (2.2)$$

Where component ‘a’ is HA, component ‘b’ is ZrO_2 or B_2O_3 and component ‘c’ is La_2O_3. Relative densities of the compositions were then calculated by comparing the measured densities with theoretical density of pure HA.

2.5.1.2 X-ray Diffraction Analysis

X-ray diffraction analysis was performed on the samples to determine presence of different phases of them using Bruker D8 advanced machine. In order to perform the diffraction analysis Cu-K_α radiation at 40kV/40 mA was used and samples were scanned in the range of 20º to 70º in 2θ with 2.0º/min resolution. The results attained from the test were compared with the Joint Committee on Powder Diffraction Standards (JCPDS) to determine the positions of the diffracted planes.

2.5.1.3 Scanning Electron Microscopy

Scanning electron microscopy was used to study the morphology and average grain size of the samples. SEM analysis was done via a LEO 1430VP equipment at a voltage of 15kV. The intercept method was used to calculate the average grain size from the SEM images [88].

$$G_{av} = \frac{L}{N \times M} \qquad (2.3)$$

Where; G_{av} is average grain size, L is circumference to the calculation circle, M is the magnification of the obtained image.

2.5.1.4 Fourier Transform Infrared Spectroscopy-Attenuated Total Reflectance

In order to identify the presence of different bonds in the composites, the FTIR-ATR spectra were used. First, the diamond plate was cleaned with a solvent (water, methanol or isopropanol) soaked with piece of tissue paper and an infrared

background was collected in order to check the clarity of the crystal. Then the solid sample was placed on the crystal and pressure was applied in order to obtain the best surface contact with the sample and the infrared beam is then emitted onto the crystal and the surface of the sample. The spectra records were performed from 4000 cm^{-1} to 400 cm^{-1} via Bruker IFS66/S.

2.5.1.5 Energy Dispersive X-ray Spectroscopy

Energy dispersive X-ray spectroscopy (EDX or EDS) identifies elemental compositions of materials imaged in a scanning electron microscope. EDX analysis system works as an integrated part of a SEM and does not operate without it. By the help of the EDX spectrum, quantitative and qualitative analysis of the elements present in the samples are performed.

In this study, EDX spectrometer that is connected to the LEO 1430VP scanning electron microscope was used for the chemical characterization of the synthesized material.

2.5.1.6 Mercury Intrusion Porosimetry (MIP)

In this method, samples that are being analyzed through possess cylindrical pores so the liquid penetration into small pores follows the capillary law.

The capillary law for a non-wetting fluid like mercury is as follows:

$$D = -\frac{4\gamma\cos\theta}{p} \qquad (2.4)$$

Where D is pore diameter (nm), p is the applied pressure (psi), γ is the fluid surface tension (mJm^{-2}) and θ is the contact angle between the solid and fluid. Since the shape of pores are rarely cylindrical, this formula is the best-fit approximation to what otherwise would be a very complex problem to solve.

To measure the volume of mercury intruded into the sample, the mercury intrusion porosimeter measures the electrical capacitance in the stem of the penetrometer. This stem is covered in metallic paint and each penetrometer is individually calibrated to give a linear relationship between volume intruded and capacitance. Porosity data presented in this thesis are obtained via automated Micrometrics Autopore IV 9520 device and are subjected to a pressure range of 50-60000 psi which can give measurements for pores of radii from 3 nm to 360 μm.

SEM images were obtained from the fractured surfaces of the samples in order to investigate the shape of the pores and their interconnectivity.

2.5.2 Mechanical Tests

2.5.2.1 Vickers Micro-hardness

The Vickers micro-hardness measurements were determined using a Vickers micro hardness tester (HMV-2, Shimadzu, Japan). Approximately 20 measurements were performed on each sample with a diamond indenter at 1.968 N load for 20 seconds. The average μ-hardness was calculated by the formula below:

$$HV = 0.001854\frac{P}{d^2} \qquad (2.5)$$

Where HV is the value of micro hardness (GPa), P stands for the amount of load (N) applied on the sample and d is the diagonal indent length (mm).

2.5.2.2 Diametral Strength

Diametral tensile strength of sintered discs was performed by a universal testing machine (LS 500; Lloyd Instruments, UK). In order to measure the diametral tensile strength, discs were located between two flat plates and compression was applied by a cylinder with a speed of 3 mm/min. During the compression, a maximum tensile

strength was generated across the flat surface diameters of the discs normal to the loading direction.

The tensile strength of the samples was calculated by the following formula [89,90]:

$$S = \frac{2F}{(\pi . D . t)} \qquad (2.6)$$

Where F stands for failure force, D stands for diameter of the sample and t is the thickness of the sample.

2.5.2.3 Drilling Test

In order to evaluate the machinability of the specimens, drilling test was performed on the pellets. The machining device was a 3-axis system with a spindle speed of 600 rpm. A 0.05 inch twist drill bit was used to perform the test on the samples.

2.5.3 Biological Characterizations

In order to investigate attachment and proliferation of the cells on pure HA and HA composite discs, Saos-2 cell line was used for in vitro cell culture experiments. After sintering at 1100ºC for 1h and then sterilizing at 200ºC for 2h, cells were seeded on all composite discs. The Saos-2 cells were grown in high glucose DMEM supplemented with 10% FBS and 0.3% Penicillin-Streptomycin. The initial cell seeding density was 5×10^4 cells/disc. The cells were incubated on composite discs in a carbon dioxide incubator (5215, Shell Lab, USA) at 37ºC under 5% CO_2 humidified environment. The medium was refreshed every 2 days. Proliferation of the cells on the discs was analyzed by PrestoBlue™ viability assay at different incubation periods. On each of the designated time points, PrestoBlue™ viability reagent was added to wells containing cell seeded discs and then the well plates were incubated at 37ºC under 5% CO_2 environment for 20h. During incubation

PrestoBlue™ reagent was reduced into intensely colored formazan, as a result of enzymatic activity of the viable cells.

After 20h of incubation, the medium in each well was collected and their absorbance was read by μQuant™ spectrophotometer (Biotek Instruments Inc., USA) with an excitation wavelength of 570 nm and emission wavelength of 600 nm. The amount of metabolic reduction caused by cells were then calculated as % reduction using the following formula provided by the manufacturer:

$$\text{Percent Reduction} = \frac{(\text{O2} \times \text{A1}) - (\text{O1} \times \text{A2})}{(\text{R1} \times \text{N2}) - (\text{R2} \times \text{N1})} \qquad (2.7)$$

Where O1 stands for molar extinction coefficient of oxidized PrestoBlue™ reagent at 570 nm, O2 stands for molar extinction coefficient of oxidized PrestoBlue™ reagent at 600 nm, R1 stands for molar extinction coefficient of reduced PrestoBlue™ reagent at 570 nm, R2 stands for molar extinction coefficient of reduced PrestoBlue™ reagent at 600 nm, A1 is the absorbance of test wells at 570 nm, A2 is the absorbance of test wells at 600 nm, N1 is the absorbance of media only wells at 570 nm and N2 is the absorbance of test wells at 600 nm. After collection the medium, cells were washed with PBS once more and growth medium was added for further culturing of cells. All experiments were run in quadruplicate and cell adhesion was evaluated based on the mean number of adherent cells. Numerical data were analyzed using standard analysis of variance (one-way ANOVA) techniques and statistical significance was considered at $p<0.05$.

2.5.3.2 Morphology of Cells

In order to investigate the morphology of Saos-2 cells on composite discs SEM analysis was performed. Two samples of each composition were seeded with cell at a seeding density of 5×10^4 cells/disc. After 1 and 7 days of incubation, the medium was removed and cells were washed with PBS and then fixed with 3% gluteraldehyde in PB for 15 minutes. Following fixation, cells were washed with PBS again and then dehydrated with graded ethanol-water solution series (30, 50, 70,

80, 90 and 100%). Following dehydration in ethanol series the discs were immersed in hexamethyldisilazane (HMDS) in order to achieve further dehydration and higher conductivity in SEM analysis and then dried in laminar flow. Prior to SEM analysis, discs were coated with gold-palladium via a precision etching coating system (PECS, Gatan 682, USA) at a thickness of 5 nm.

CHAPTER 3

RESULTS and DISCUSSION

3.1 Density of the samples

Densities of the samples after the sintering process at 1100ºC for 1h are presented in Table 3.1.

Table 3.1: Density values of the materials sintered at 1100ºC for 1h.

Group ID	Sample ID	Sintered Density (g/cm^3)	Theoretical Maximum Density (g/cm^3)	Relative Density (%)
Group 1	Pure HA	2.91	3.15	92.2
	90HA10Zr	3.14	3.30	95.2
	88HA10Zr2La	2.93	3.35	87.4
	80HA20Zr	3.02	3.48	86.7
	78HA20Zr2La	2.74	3.51	78.06
Group 2	90HA10B	2.82	3.15	89.5
	88HA10B2La	2.75	3.19	86.2
	80HA20B	2.33	3.15	74.0
	78HA20B2La	2.41	3.18	75.7

In Table 3.1, relative density of all samples decreased by addition of La_2O_3. However, for sample 78HA20B2La which showed a 1.7% increase in relative density in comparison to sample 80HA20B. Sample 90HA10Zr had the highest relative density among others after the sintering at 1100ºC for 1 h.

It was also observed that samples 90HA10Zr and 90HA10B possess the highest density values in Groups 1 and 2, respectively. Results showed that in samples of Group 1, relative density of the samples decreased as the amount of ZrO_2 increased in the composites. Same results were obtained in samples of group 2 showing a decrease in density of the samples as the amount of B_2O_3 present in the composites increased. It was also observed that the density of the samples of group 1 including ZrO_2 and La_2O_3 as additional powders was notably higher than that of the samples of group 2 having B_2O_3 and La_2O_3 as additional powders.

It was reported that addition of ZrO_2 resulted in a decrease in the density of the composites [38]. It was reported that as the amount of ZrO_2 in the composites increased, the relative densities of the samples decreased [76,91]. These results are in correlation with the obtained results of this thesis. As for the samples of Group 2, effect of the addition of B_2O_3 has been investigated in several studies. It was reported that addition of B_2O_3 to HA composites enhanced the mechanical properties of the composites. However, in most of the conducted studies, samples were prepared in nanotube structure, which enhances the mechanical properties of the samples noticeably regardless of other factors involved [85,92,93,94]. Despite the fact that several studies have analyzed the effect of addition of compounds of B_2O_3, no work has been done to determine and compare the effect of addition of La_2O_3 on the density of HA and B_2O_3 composites.

In another study, the effect of incorporation of La_2O_3 to HA was investigated. It was reported that addition of La_2O_3 has a positive effect on density of the samples at high sintering temperatures (>1300ºC). However, it was reported that it is not possible to draw a firm conclusion regarding the effect of La_2O_3 on mechanical properties of HA composites at lower temperatures [95]. It was reported that increasing the porosity in HA composites with ZrO_2 was a result of produced water in the

decomposition of HA which is trapped in the pores shaped in the sintering process resulting in decreased density of the samples which was in correlation with the results of this study [38].

3.2 Structural Analysis

3.2.1 X-ray Diffraction Analysis

Presence of different phases in the samples was investigated via conducting the XRD analysis. XRD result of the pure HA sintered at 1100ºC for 1 h is presented in Figure 3.1. Peaks are corresponding to pure HA. No secondary phases were observed in this XRD pattern.

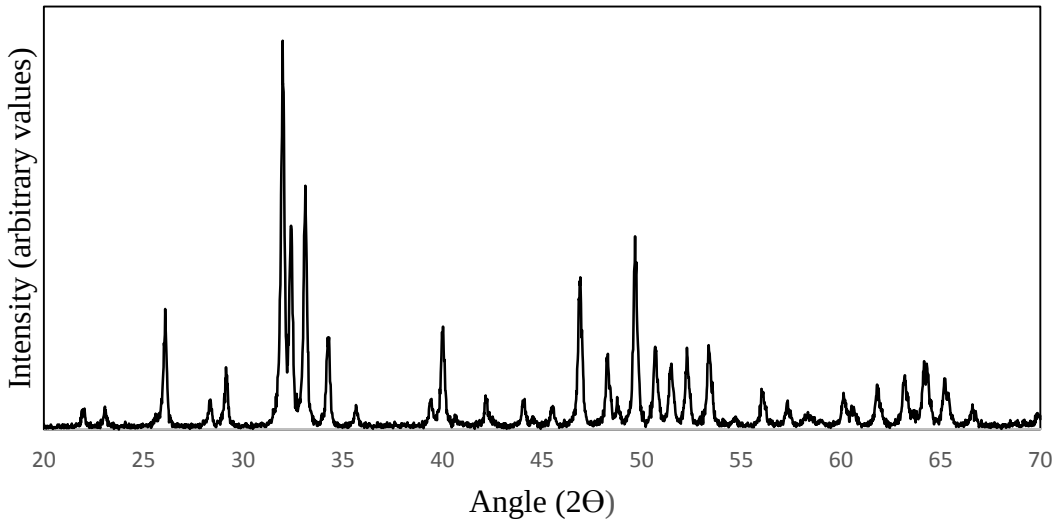

Figure 3.1: XRD pattern of pure HA sintered at 1100ºC for 1h.

Reference patterns for the materials used in the composites are presented in Figure 3.2. In this figure, peaks representing different materials can overlap at different locations.

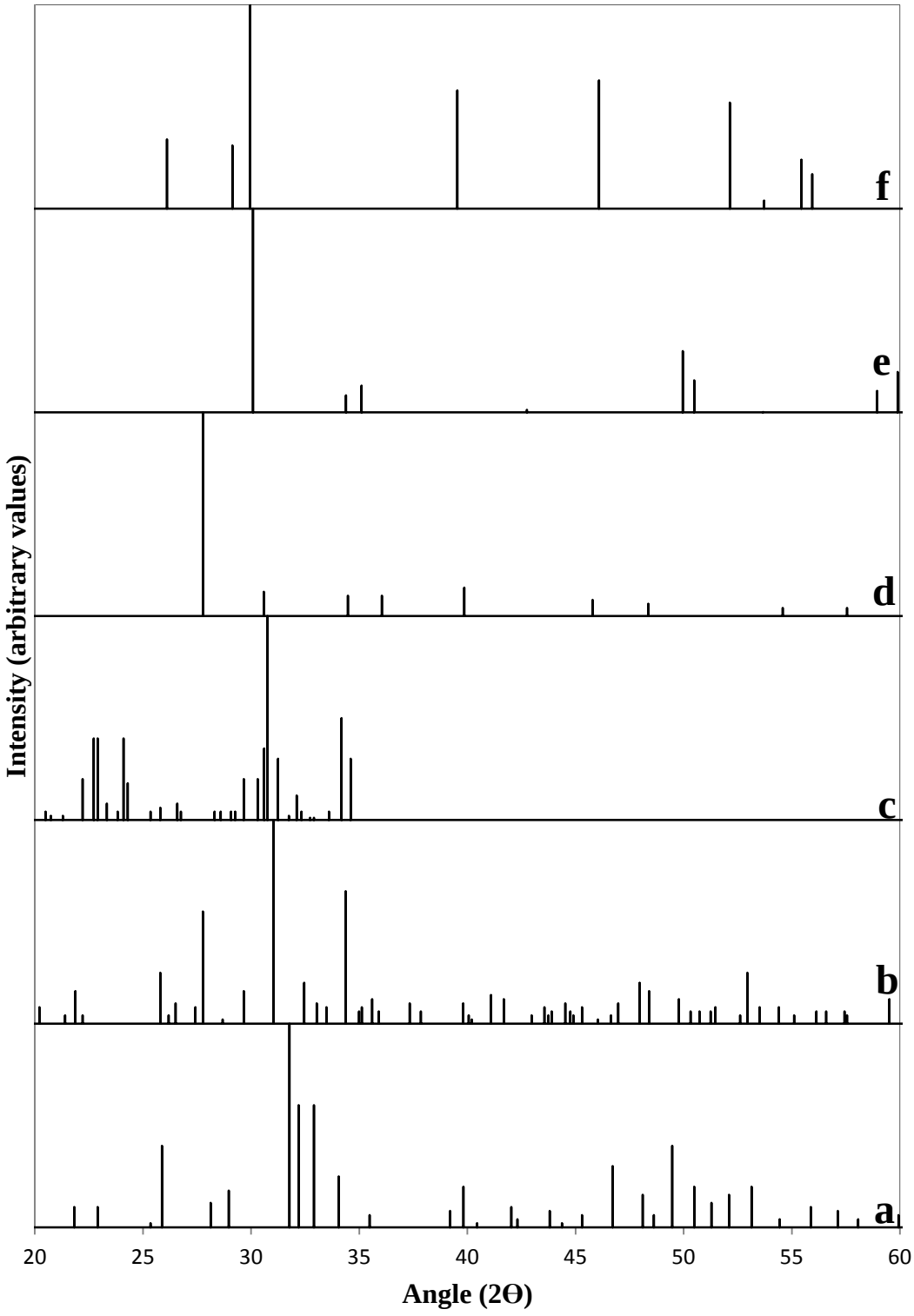

Figure 3.2: XRD patterns for a) Standard HA (JCPDS #9-432); b) Standard β-TCP (JCPDS #9-169); c) Standard α-TCP (JCPDS #9-348); d) Standard B_2O_3 (JCPDS #06-0297); e) Standard t-ZrO_2 (JCPDS #17-923); f) Standard La_2O_3 (JCPDS #05-0602)

Figures 3.3 and 3.4 present the diffraction patterns for composites of Groups 1 and 2, respectively. According to the results illustrated in Figures 3.3 and 3.4, the composite patterns had the XRD pattern belonging to HA (JCPDS #9-432). Results revealed that the peaks corresponding to presence of different phases in the composites are narrow indicating that the composites are highly crystalline.

In Figure 3.3, overlapping peaks at various locations were observed for different phases of ZrO_2, making it difficult to distinguish between peaks belonging to tetragonal phase with those of cubic phase. HA decomposes to β-TCP at lower temperatures in the presence of t-ZrO_2 and forms CaO. On the other hand, CaO dissolves into the structure of t-ZrO_2 and results in its decomposition as well, which in turn leads to formation of c-ZrO_2 and $CaZrO_3$ as a second phase.

In sample 90HA10Zr, it was observed that intensity of the peaks was lower in comparison to that of pure HA. Peaks belonging to t-ZrO_2 were observed. Also, as a secondary phase, c-ZrO_2 peaks were observed occurring very close to those of t-ZrO_2 and very small amount of $CaZrO_3$ was observed as well. As for the second sample of 88HA10Zr2La, the overall intensity of the peaks was decreased in comparison to that of pure HA and 90HA10Zr. Peaks representing t-ZrO_2 and La_2O_3 were observed. Second phases were present as c-ZrO_2 and very small amount of $CaZrO_3$. In 80HA20Zr, there exists a decrease in the intensity of the peaks in comparison to that of pure HA. Addition of ZrO_2 content in the sample in comparison to sample 90HA10Zr was visible at peak $2\theta = 30.21^o$ corresponding to ZrO_2. Peaks corresponding to c-ZrO_2 and $CaZrO_3$ as secondary phases were also present. In 78HA20Zr2La, peaks had lower intensities in comparison to those of pure HA and as a result of incorporation of La_2O_3 the intensities were lower in comparison to 80HA20Zr sample. Also, addition of ZrO_2 in comparison to 88HA10Zr2La sample was visible at $2\theta = 30.25^o$.

Presence of secondary phases in the resulting composition can occur as a result of synthesis method used, which had a high pH value and also aging time and temperature [96].

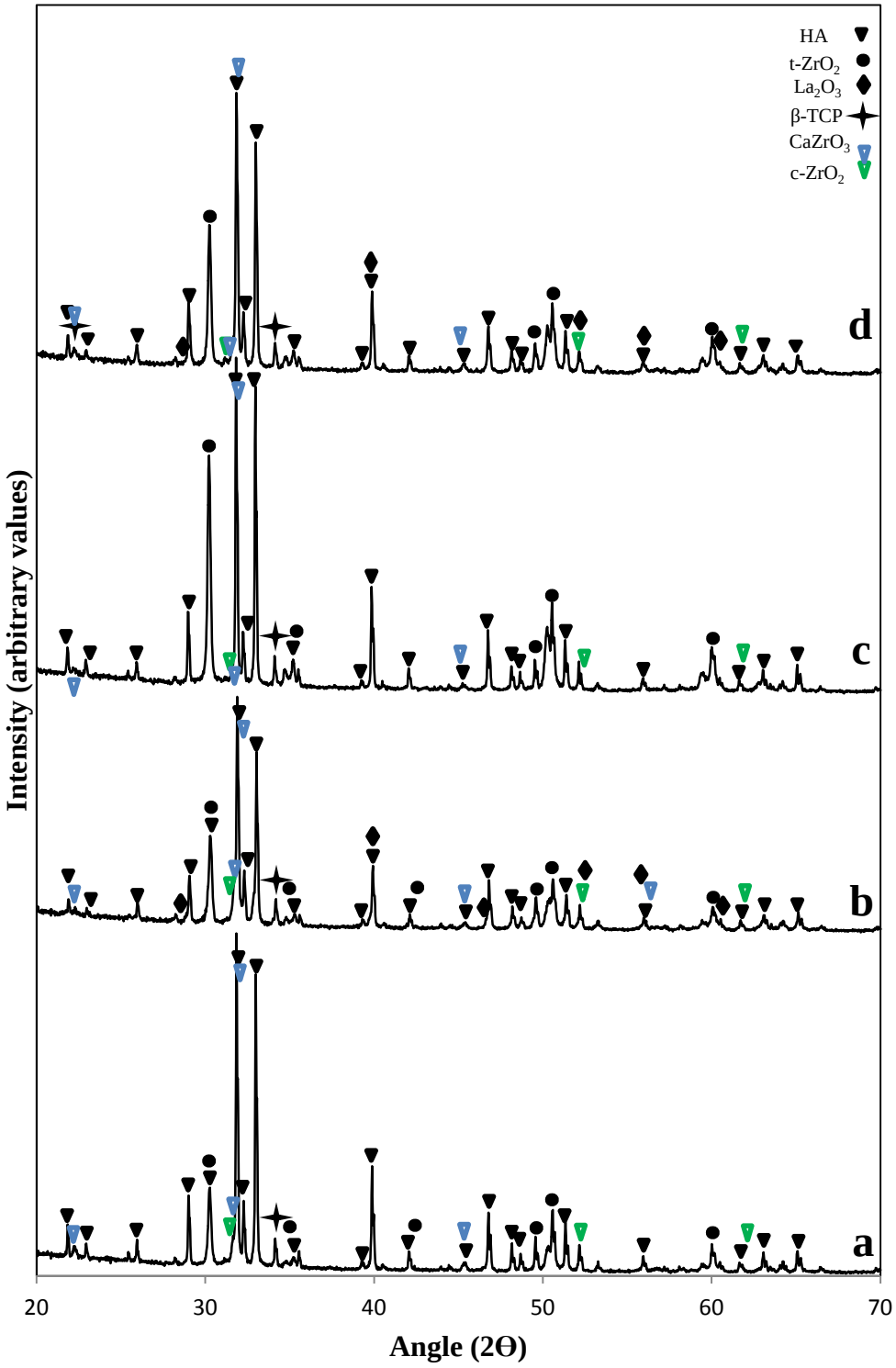

Figure 3.3: XRD patterns of a) 90HA10Zr; b) 88HA10Zr2La; c) 80HA20Zr; d) 78HA20Zr2La sintered at 1100ºC for 1 h.

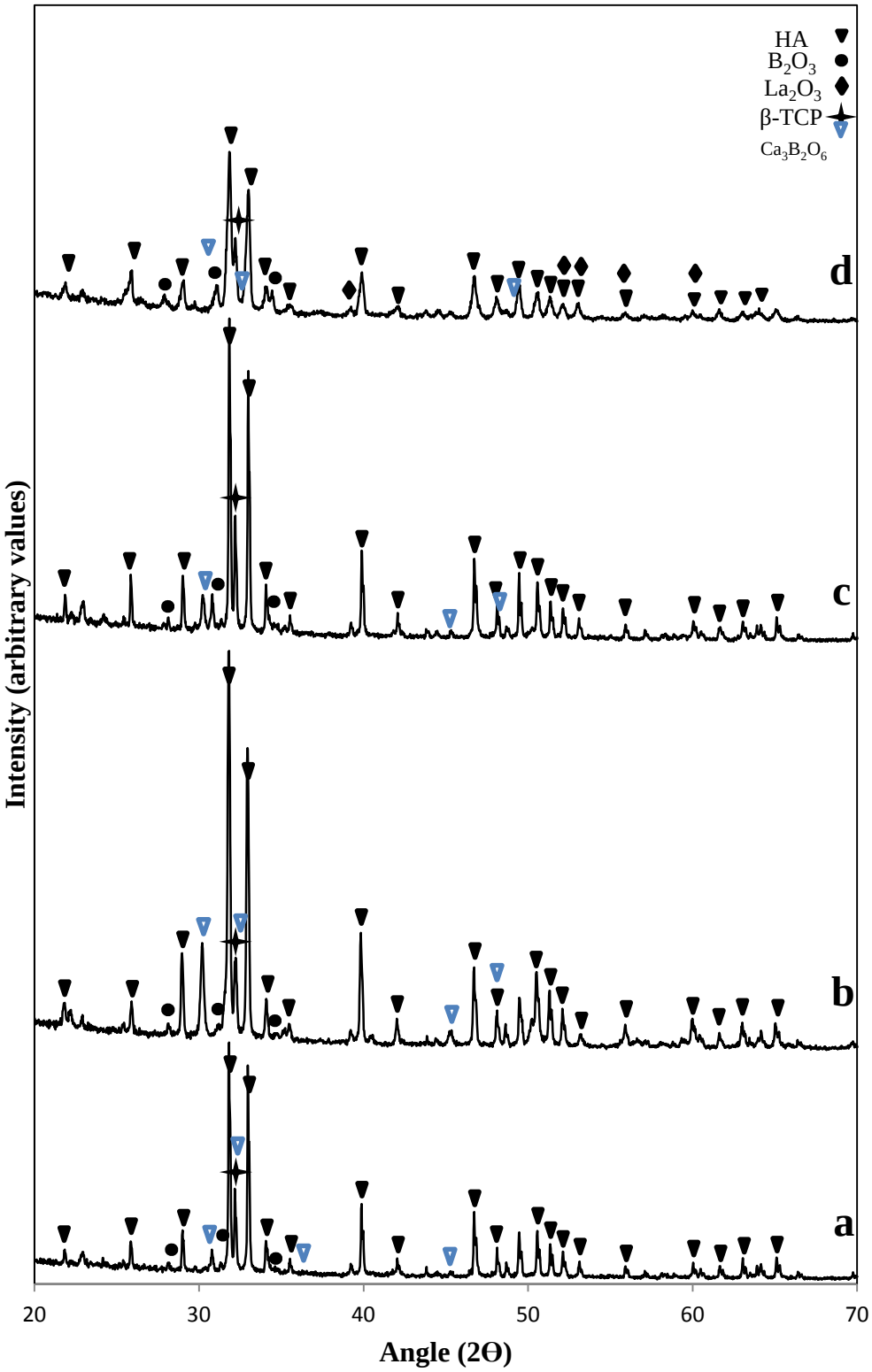

Figure 3.4: XRD patterns of a) 90HA10B; b) 88HA10B2La; c) 80HA20B; d) 78HA20B2La sintered at 1100ºC for 1 h.

Decrease in the intensity of peaks in composites including La_2O_3 in comparison with those including only ZrO_2, suggests that presence of La_2O_3 in the composition leads to further consumption of HA. XRD patterns of group 1 also showed a slight shift to the left in their corresponding peak values.

Obtained patterns show clear and sharp peaks associated with HA suggesting that the produced materials were highly crystalline and possessed high purity. As expected, peaks representing α-TCP were not present indicating that decomposition of HA did not advance further because of the sintering temperature. These results are in correlation with the investigation of Rapacz-Kmita et al. [77] and Heimann et al. [97].

However, addition of the ZrO_2, B_2O_3 or La_2O_3 into HA did not result in much of a change in XRD patterns of the HA and they were still matching with the standard JCPDS file for HA.

Figure 3.4 presents the diffraction patterns obtained for composites of group 2. It was observed that the intensity of all peaks decreased in comparison with that of pure HA suggesting the involvement of HA in reaction with other composite powders.

It was observed that for sample of 90HA10B, intensity of the peaks decreased in comparison to that of pure HA and as secondary phases of $Ca_3B_2O_6$ were observed in this sample. As for 88HA10B2La sample, the intensity of the peaks was decreased in comparison to that of pure HA and like the first sample $Ca_3B_2O_6$ secondary phases was observed in this sample. In 80HA20B sample, there was a decrease in the intensity of the peaks in comparison to peaks of pure HA. Also it was observed that peaks corresponding to HA slightly increased in this sample comparing to 90HA10B sample. As for the 78HA20B2La sample, it was observed that like other samples in group 2 the intensity of peaks decreased in comparison to pure HA, and also there was a notable decrease in intensity of the peaks as the amount of B_2O_3 content increases in the composite comparing to 88HA10B2La sample.

The slight increase in the intensity of the peaks corresponding to HA in 80HA20B sample comparing to that of 90HA10B sample suggests that increasing the amount of B_2O_3, reduces decomposition rate of HA.

Also, noticeable decrease in intensity of the peaks of 78HA20B2La sample comparing to 88HA10B2La sample suggests that the amount of the incorporated B_2O_3 and La_2O_3 together was important in decomposition of HA which was in correlation with the findings of Ergun et al. [98]. In another study, decomposition of composites of HA and La_2O_3 was observed despite the fact that sintering temperature was below the intrinsic decomposition of HA (1300ºC). It was reported that the decomposition was probably a result of reaction between HA and La [98]. The major peaks in this set of patterns belong to HA and some low intensity peaks belonging to B_2O_3 are present. Also in all of the samples of group 2, it was observed that some of the peaks belonging to B_2O_3 overlap with HA peaks in vicinity and that none of the main peaks corresponding to α-TCP was observed in XRD patterns of composites of B_2O_3 and HA, indicating that HA did not decompose completely which was in correlation with our results [85].

It was also reported that absence of any important peak in the XRD pattern indicates that no noticeable amount of chemical impurities were present in the as-received B_2O_3 powder [92]. XRD patterns of composites of group 2 also showed a slight shift to the left in their corresponding peak values.

3.2.2 Fourier Transform Infrared Spectroscopy Results

FTIR tests were conducted on the samples in order to determine the existence of different chemical bonds in the composites. Table 3.2 presents the FTIR spectra values for different bonds in the structure of the HA and their assignments.

Table 3.2: Frequencies and assignments of the FTIR bands in HA in 4000-400 cm^{-1} region.

Functional Group	Vibration Mode	Infrared Wavenumber (cm^{-1})	Ref. No.
$(PO_4)^{3-}$	ν_1	962	92
$(PO_4)^{3-}$	ν_2	474	92
$(PO_4)^{3-}$	ν_3	1046,1087	92
$(PO_4)^{3-}$	ν_4	571,601	92
OH^-	Librational	630	92
OH^-	Stretching	3572	92

Figure 3.5 presents FTIR spectra of four different composites of group 1. According to this figure, there was a decrease in the intensity of the OH^- stretching band as the amount of incorporated ZrO_2 in the composite increased, which a sign of decomposition is of HA as a result of presence of ZrO_2. Normally, the decomposition of HA occurs at around 1300ºC but with ZrO_2 present this temperature drops to approximately 900ºC alongside formation of β-TCP [99]. This reaction between HA and ZrO_2 results in production of $CaZrO_3$, however, the bands associated with the compound were not observed which might be because of the lack of CaO produced in the decomposition reaction of HA or because all of the produced CaO has been dissolved into ZrO_2 [99]. Presence of CaO was reported to be very disadvantageous in compounds that are used as implant materials due to its high reaction drive with water [100].

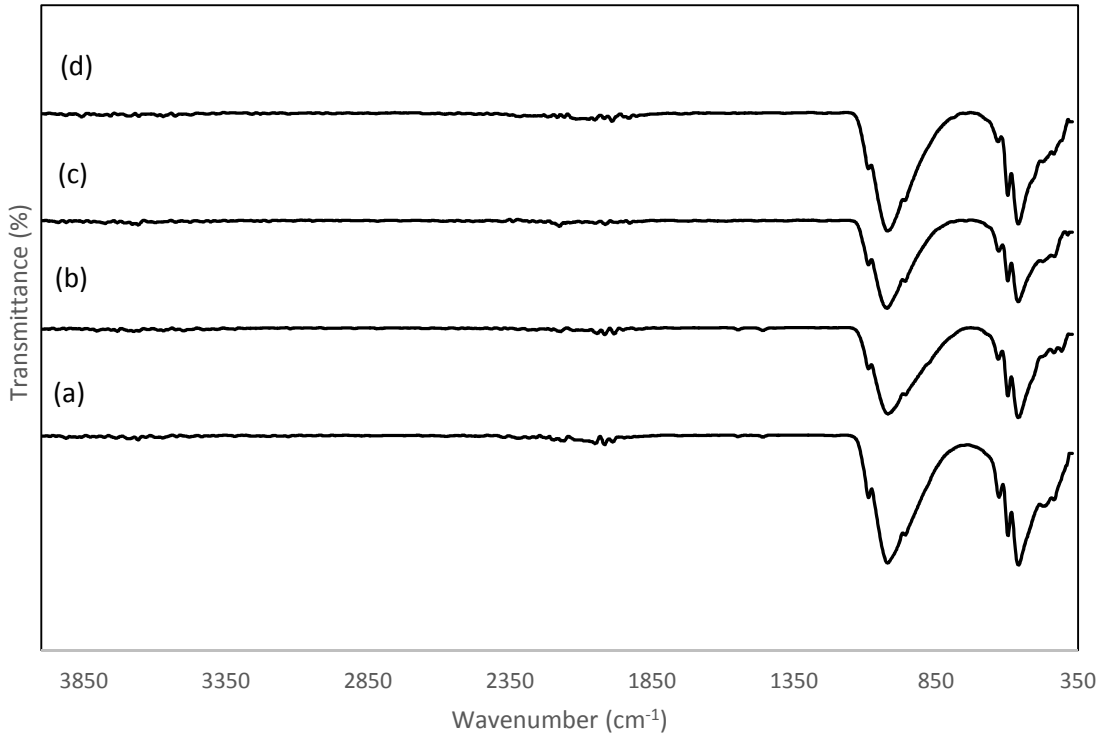

Figure 3.5: FTIR spectra of a) 90HA10Zr; b) 88HA10Zr2La; c) 80HA20Zr; d) 78HA20Zr2La sintered for 1h.

Table 3.3 presents the location of the corresponding bands in different composites of group 1.

Table 3.3: Locations of the bands observed in compositions of group 1.

	ν_2	ν_4	OH^- Lib	ν_1	ν_3	OH^- Stretching
Pure HA	474	571,601	630	9628	1046,1087	3572
90HA10Zr	472	559,596	628	958	1020,1087	3573
88HA10Zr2La	474	559,597	630	957	1019,1087	3569
80HA20Zr	474	560,597	628	958	1023,1087	3569
78HA20Zr2La	474	559,597	631	959	1020,1087	3566

In addition to the characteristic peaks corresponding to PO_4^{3-} ions stretching and deformation vibration, a small low intensity peak at 1460 cm^{-1} was observed which is related to the CO_3^{2-} group, which in turn, may be the result of the ambient air atmosphere during the synthesis reaction [99]. The peak observed at 3572 cm^{-1} was pretained to the stretching mode of OH^- ions. A gradual decrease in the intensity of the OH^- band was observed which indicates the partial dehydration of the HA as a result of addition of ZrO_2, which in turn, causes β-TCP to form [99]. There was also a peak observed at approximately 434 cm^{-1} which is associated with ZrO_2 and confirms the presence of ZrO_2 in the structure of the composite. As for the trace amount of lanthanum, the bands observed at around 3500 cm^{-1} which pertained to the existing water in the composition and the bands observed at 630 and 3572 cm^{-1} were the evidence of good crystallinity for the HA and La composites [101].

In Figure 3.6, FTIR spectra of four different composites of group 2 was presented. Even though there exists some IR spectra studies pertaining to borate and phosphate compounds, very little studies conducted on borohydroxyapatites are present in the literature. Beside the characterization peaks coming from HA, as seen in Table 3.4, presence of bands associated to borate groups vibrations were also observed. Bands related to both BO_3^{3-} and linear BO_2^- is observed in the FTIR spectra of compositions of group 2. The bands at 742 and 780 cm^{-1} and bands observed at 1205 and 1245 cm^{-1} are attributed to symmetric bending ν_2 and asymmetric stretching ν_3 mode of BO_3^{3-} group. Also, a small peak was observed at 1930 cm^{-1} which is related to the asymmetric stretching of ν_3 mode of linear BO_2^- group [102].

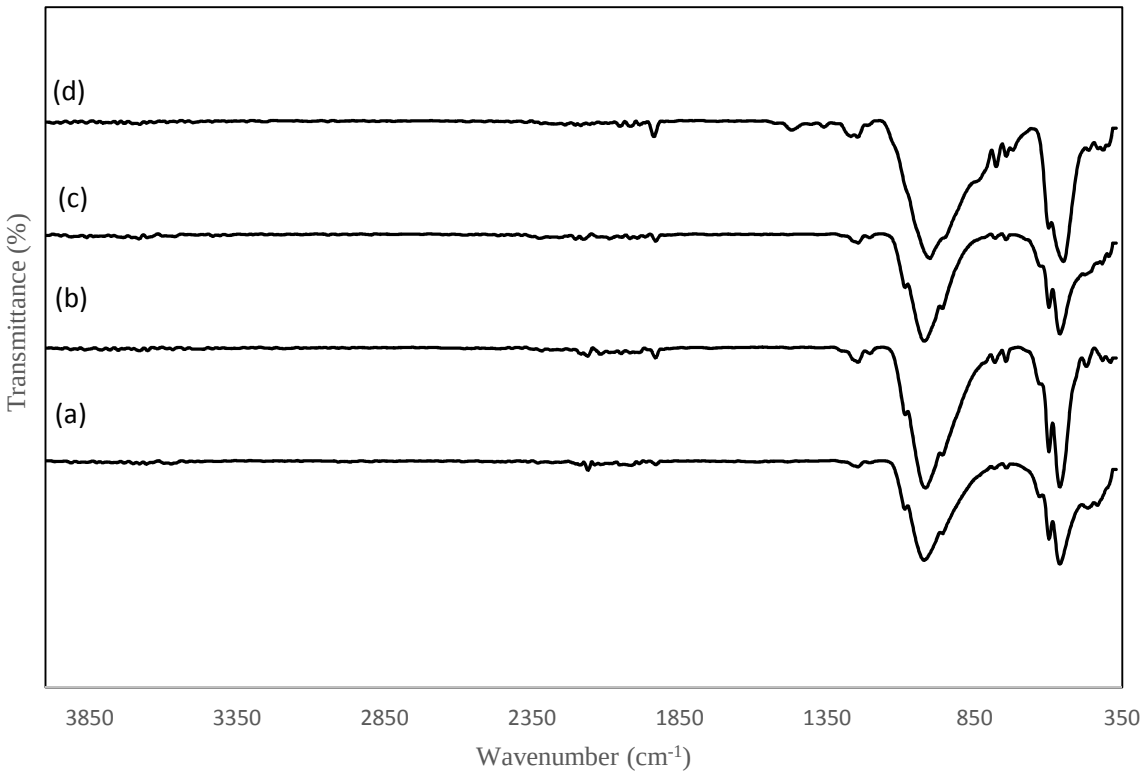

Figure 3.6: FTIR spectra of a) 90HA10B; b) 88HA10B2La; c) 80HA20B; d) 78HA20B2La sintered for 1h.

Table 3.4 presents the location of the known bands in composites of group 2.

Table 3.4: Locations of the bands observed in composites of group 2.

	ν_2	ν_4	OH^- Lib	ν_1	ν_3	OH^- Stretching
Pure HA	474	571,601	630	9628	1046,1087	3572
90HA10B	476	561,598	626	959	1020,1085	3561
88HA10B2La	471	561,598	628	958	1016,1085	3567
80HA20B	476	561,598	626	959	1020,1085	3561
78HA20B2La	463	549,598	-	949	1002, -	3553

In the IR spectra the characteristic band location for the OH^- group was observed at 3572 cm^{-1}, but with increasing amount of B_2O_3 in the composition a second band appeared at 1930 cm^{-1} pertaining to $Ca(OH)_2$ which was considered an impurity according to literature [102]. Addition of La_2O_3 to the composition had different effects on the FTIR spectra of the compositions. The band at 471 cm^{-1} related to ν_2 stretching of PO_4^{3-} group of 88HA10B2La showed a noticeable decrease in the intensity of the peak. Also the bands at 742 and 777 cm^{-1} showed a noticeable increase in the intensity with a little shift to the right in 777 cm^{-1} band. Also the ν_1 band corresponding to the PO_4^{3-} of HA was shifted to right and had a peak of higher intensity. It was observed that increasing the amount of B_2O_3 whilst having La_2O_3 in the composition elements caused the disappearance of the bands at 630 cm^{-1} corresponding to OH^- libration and the band at 1085 cm^{-1} corresponding to ν_3 mode of the PO_4^{3-} group. Also, the band pertaining to the OH^- stretching was shifted to right and identified at 3553 cm^{-1}.

3.2.3 Energy Dispersive X-ray Spectroscopy

EDX was conducted on the samples in order to determine presence and the weight percentage of different atoms present in the structure of the composites. EDX spectrum of the samples sintered at 1100ºC for 1 h are presented in Figures 3.7-3-8. These figures show the general analysis of the surface of the material. Atoms of oxygen, phosphorous, calcium, zirconium, lanthanum and gold were observed in the spectrum of different composites. Because oxygen was adsorbed on the surface of the material, O_2 atoms were observed in the spectrum. Au atoms present in the spectrum are originated from the coating of the material surface which increases conductivity.

It was observed that all composites have either lower or higher Ca/P ratio than that of theoretical HA which is expected since EDX obtains the data from a single point on the surface of the sample and since the Ca/P ratio distribution pattern is not uniform, such results are expected [103]. In Figure 3.7, EDX spectrum of the composites including ZrO_2 and La_2O_3 are presented. It was observed that in all four

composites the Ca/P ratio was higher than the theoretical Ca/P ratio of HA, which suggests that the structure of HA in that specific part of the sample was more rich in calcium than phosphorus. It was also reported that the higher Ca/P ratio in HA undergoing sintering can result in calcium-derived compounds such as CaO, $Ca(OH)_2$ and $CaCO_3$ or a mixture of all three [103].

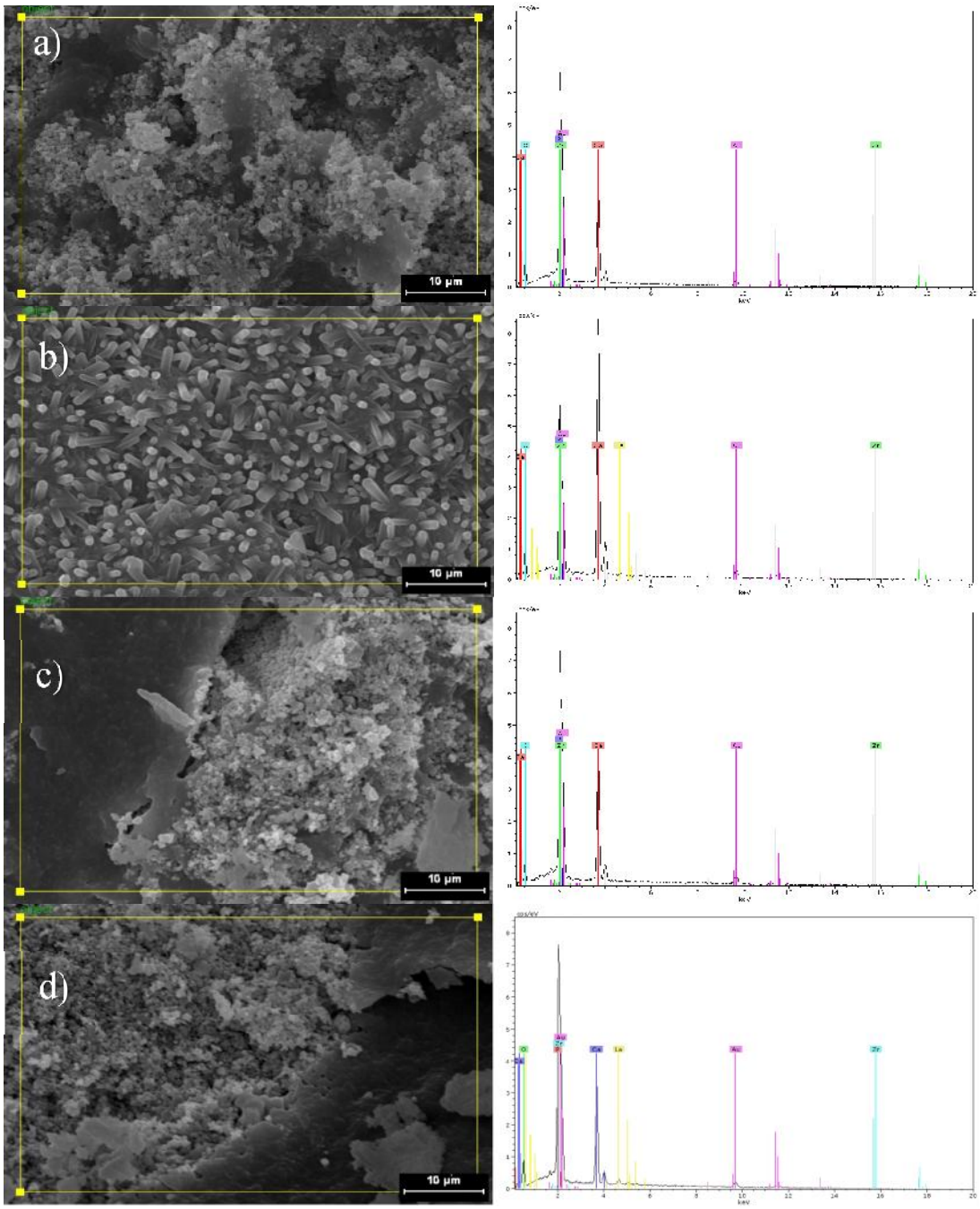

Figure 3.7: EDX spectrum of a) 90HA10Zr; b) 88HA10Zr2La; c) 80HA20Zr; d) 78HA20Zr2La sintered at 1100ºC for 1h.

The obtained results prove that there were no impurities present in the structure of the samples. Traces of the oxygen atom present in the samples, were also observed in the HA powder used as starting material [104].

EDX spectrum of samples of the composites including B_2O_3 and La_2O_3 are presented in Figure 3.8. Peaks corresponding to B_2O_3 are not visible in these spectrum since boron is a member of the light elements group and since these elements have low photon energies they lead to complications like a high absorption in the sample and in the detector which results an incorrect measurement of photons or peaks being located close to the electronic noise of the detection system (can be observed at 0KeV) and thus making it very difficult to quantify. Also EDX has a relatively poor energy resolution which leads to frequent peak overlaps as well as the inability to separate the members of the X-ray families that occur at low energy (<3KeV). The K peaks of the light elements occur in the X-ray energy range below 1KeV causing an interfere problem between them and L- and M-family peaks of heavier elements [103,104]. It was observed that in 88HA10B2La and 78HA20B2La composites, the Ca/P ratio was higher than the theoretical Ca/P ratio of HA, which is also a sign of presence of calcium-derived compounds such as CaO, $Ca(OH)_2$ and $CaCO_3$ or a mixture of all three. As for 90HA10B and 80HA20B composites it was observed that the Ca/P ratio is lower than theoretical Ca/P ratio of HA. The obtained values indicated presence of $Ca_3(PO_4)_2$ with a theoretical Ca/P ratio of 1.5 [103]. It was reported that CaO and $Ca_3(PO_4)_2$ are formed during sintering process from nonstoichiometric HA depending on the Ca/P ratio of the feed material. CaO is formed at higher and $Ca_3(PO_4)_2$ is formed at lower Ca/P ratio than 1.67 [103]. Since $Ca_3(PO_4)_2$ was present in only 2 of 8 samples it is reasonable to assume that the Ca/P ratio in the synthesized HA was somewhat higher than 1.67 [103,104].

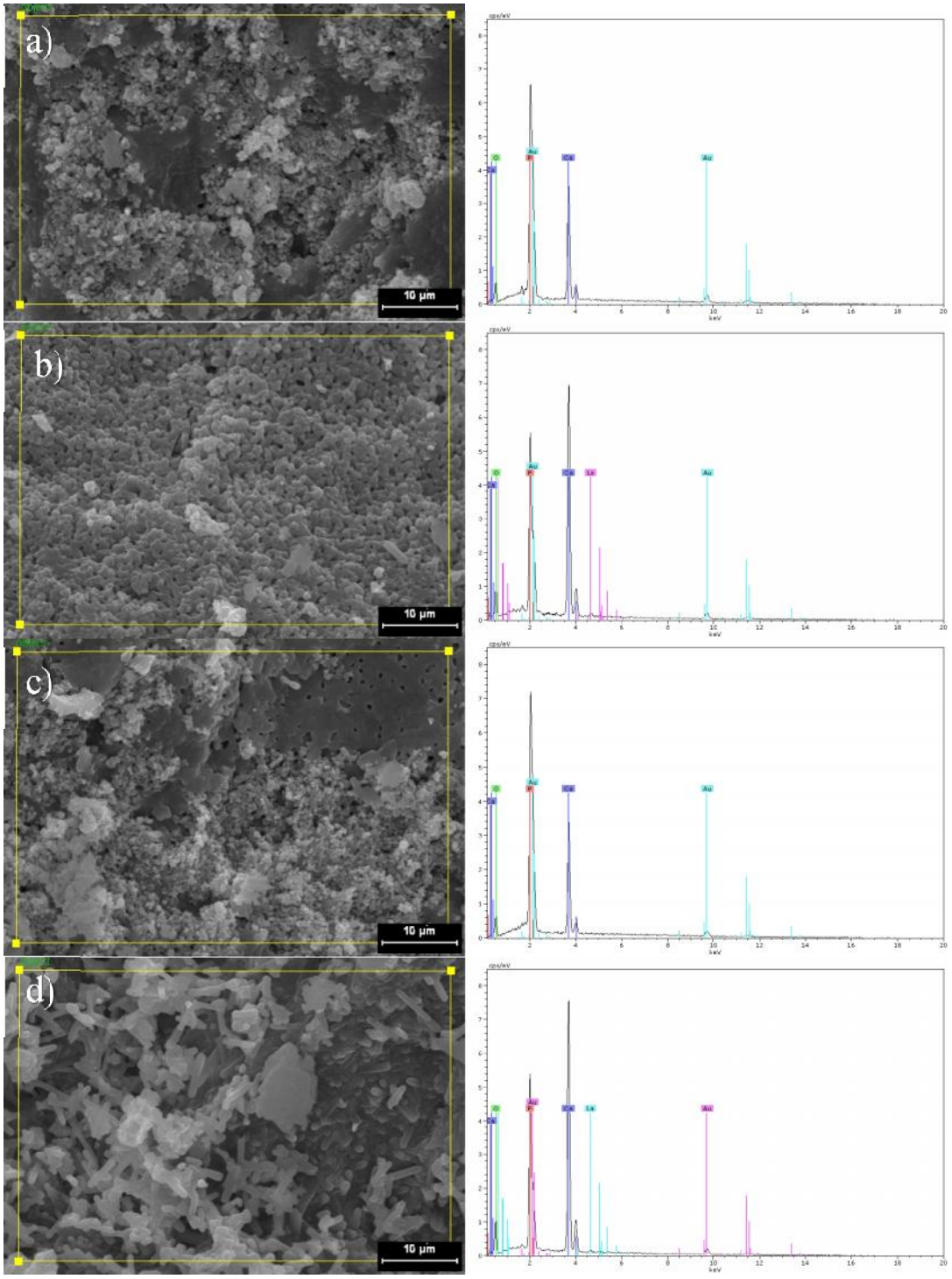

Figure 3.8: EDX spectrum of a) 90HA10B; b) 88HA10B2La; c) 80HA20B; d) 78HA20B2La sintered at 1100ºC for 1h.

The percent weight and percent atom values for the materials identified in the EDX spectrums are presented in Table 3.5.

Table 3.5: wt% and at% of materials identified in the EDX spectrum of composites sintered at 1100ºC for 1h.

	Wt %						At %					
	Ca	P	Au	Zr/B	La	O	Ca	P	Au	Zr/B	La	O
90HA10Zr	17.33	8.22	14.36	16.4	0	43.69	11.74	7.21	1.98	4.88	0	74.18
88HA10Zr2La	36.38	13.76	16.36	0.16	0.81	32.52	26.12	12.78	2.39	0.05	0.17	58.49
80HA20Zr	17.14	8.57	13.5	40.12	0	20.66	17.08	11.06	2.74	17.56	0	51.56
78HA20Zr2La	14.49	8.52	9.39	23.36	2.91	41.33	10.2	7.76	1.35	7.22	0.59	72.88
90HA10B	19.23	19.41	17.69	Unidentified	0	43.67	12.22	15.96	2.29	Unidentified	0	69.52
88HA10B2La	31.13	14.82	18.22	Unidentified	0.42	35.4	21.8	13.42	2.6	Unidentified	0.09	62.1
80HA20B	16.7	21.82	8.76	Unidentified	0	52.72	9.34	15.8	1	Unidentified	0	73.87
78HA20B2La	35.66	14.27	12.93	Unidentified	0.92	36.22	24.14	12.5	1.78	Unidentified	0.18	61.41

3.2.4 Mercury Intrusion Porosimetry (MIP)

Mercury intrusion porosimetry test was conducted on samples in order to determine percent porosity of composites. In Table 3.6, the porosity values and average pore diameters obtained by mercury intrusion method and ratio of bulk or measured density to density obtained by mercury intrusion method are presented.

Table 3.6: Porosity measurements for samples sintered at 1100ºC for 1h.

	% Porosity	Average Pore Diameter (4V/A)	Bulk Density/ MIP Density
Pure HA	8.53	14856 A	1
90HA10Zr	2.26	37321 A	0.90
88HA10Zr2La	7.15	1785 A	0.95
80HA20Zr	18.38	1266 A	1.00
78HA20Zr2La	18.86	1450 A	1.00
90HA10B	12.64	6442 A	0.92
88HA10B2La	14.6	2622 A	0.98
80HA20B	21.87	1573 A	1.06
78HA20B2La	30.28	1996 A	0.79

It was observed that increasing amount of ZrO_2 or B_2O_3 increased the porosity of the composites for all samples. In case of introducing La_2O_3 into the composites, it was observed that porosity values increased for all samples which is in good agreement with density results and thus explains the relation between density and hardness values obtained in this study. Moreover, samples 78HA20B2La and 90HA10Zr possess the highest and lowest porosity values respectively, which is also in good agreement with micro-hardness and density values.

Unfortunately, there are no previous literature work done on composites of HA mixed with ZrO_2, B_2O_3 and La_2O_3.

Density plays an important role in the determination of the structure of sintered porous ceramics, and can offer information about pore distribution and size, mechanical strength, permeability and presence of structural faults [105]. A close relationship between these data was established. Low porosity coincided with a high level of densification. Porosity is a very important property since it is directly related

to presence of open pores which effects other properties such as tissue ingrowth and mechanical properties [104]. To validate the results obtained from density measurements, density of the samples were also measured via mercury intrusion porosimetry and it was observed that the ratio of bulk densities from mercury intrusion porosimetry to geometric densities has an average of 0.95±0.07 which means that they are in good agreement with each other [106]. The average pore diameter was calculated with the assumption that all the pores were cylindrical in shape. Under this geometrical condition, the average pore diameter (D) in μm equals four times the total pore volume (V) in cm^3/g divided by specific area (A) in m^2/g of the pores. The total pore volume was obtained from the porosimeter data; the surface area can be obtained from either the porosimeter data [107], as was done in this study, or from independent determination of the nitrogen (B.E.T.) adsorption isotherm which was not suitable for our samples [108].

In Figure 3.9, SEM images of the fractured surfaces of the samples are presented. These images provide various information regarding pore shape and size. SEM images showed that the porous ceramic structure obtained possess open and close pores with varying pore diameters depending on sample density.it was reported that pore shape and size analysis are crucial for structural investigation of the samples because there is a direct relationship between pore shape and osteoconductive, mechanical, permeability and dissolution properties of the porous ceramic [104]. It was also reported that interconnection and presence of open pores are very important to allow the substances flow inside the structure [105,109,110]. However, it was observed that the pores are not properly interconnected. It was reported that pore size also depends on the weight and size of the added powder materials [111,112]. It was observed that with increasing amount of ZrO_2 or La_2O_3 in samples of the first group, the grain size of the samples decrease allowing for more interconnected pores to shape. As for the case of samples including B_2O_3 or La_2O_3 in their structure it was observed that with increasing amount of the powder materials, the grain sizes increased, making the structures more porous and thus weakening the mechanical properties. These results were in good agreement with average grain size, micro-hardness and porosity results obtained in this study.

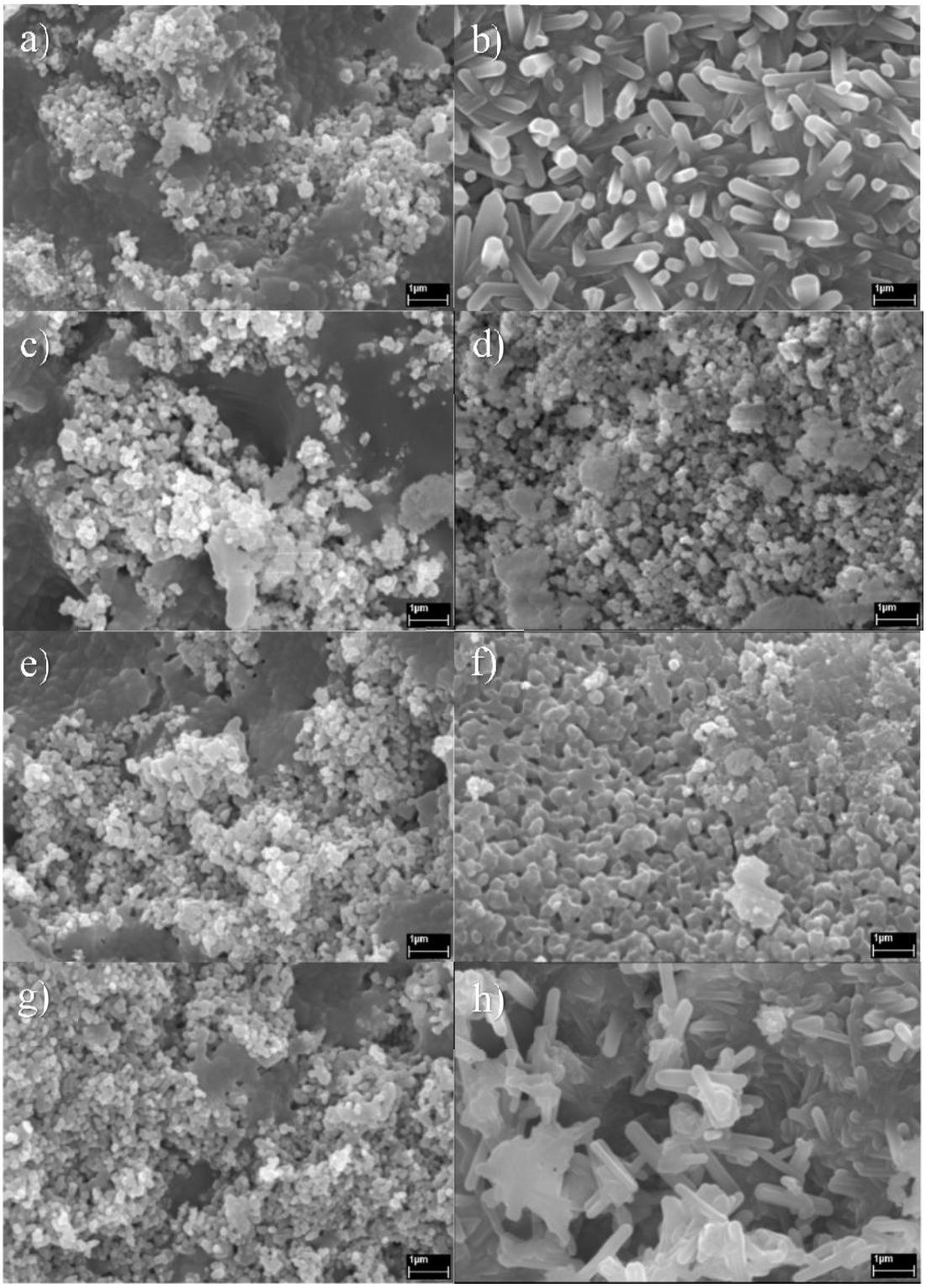

Figure 3.9: SEM images of fractured surfaces of a) 90HA10Zr; b) 88HA10Zr2La; c) 80HA20Zr; d) 78HA20Zr2La; e) 90HA10B; f) 88HA10B2La; g) 80HA20B; h) 78HA20B2La.

3.2.5 Microstructure of the Samples

Scanning electron microscopy was conducted in order to inspect the morphology of the samples. Images of the samples are presented in Figures 3.10 and 3.11. All images were taken from the surface of samples sintered at 1100ºC for 1 h. In Figure 3.10, it was observed that the grain size of the samples of group 1 decreased when compared to grain size of HA. It was observed that with increasing amount of ZrO_2 and also with the introduction of La_2O_3 into the composite, the grain size of the samples decreased.

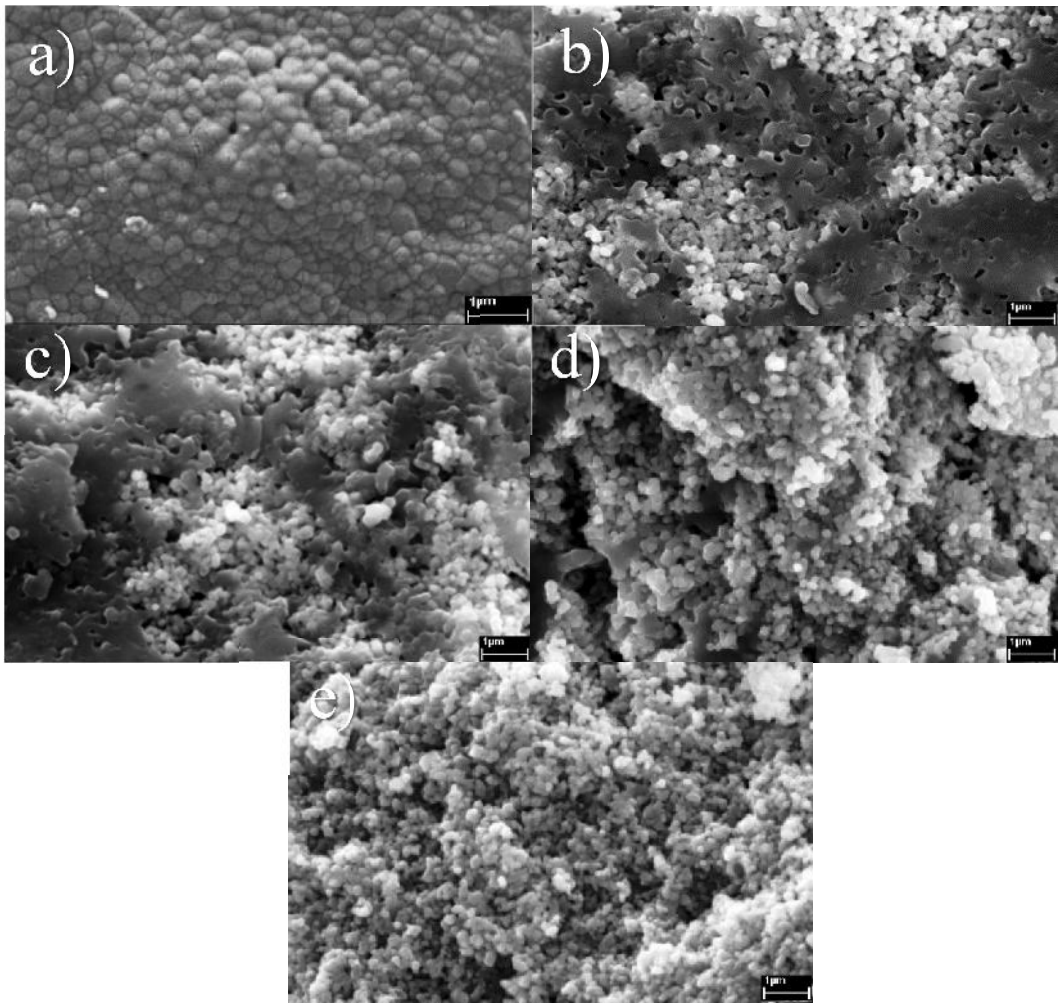

Figure 3.10: SEM images of a) Pure HA; b) 90HA10Zr; c) 88HA10Zr2La; d) 80HA20Zr; e) 78HA20Zr2La.

Figure 3.11 presents the SEM images of the samples of group 2. It was observed that with increasing amount of B_2O_3 and with introduction of La_2O_3 into the composites, the grain sizes of the samples increased, with the exception of 88HA10B2LA sample which exhibited a decrease in grain size with introduction of La_2O_3 into its composition.

Effect of doping divalent and trivalent ions into the structure of HA was examined in a recent study. Pure and doped samples were synthesized via precipitation method and sintered at 1100ºC for 1 h. It was reported that incorporation of divalent ions such as Mg^{2+} and Zn^{2+} into the structure of HA resulted in higher average grain size in comparison to pure HA. On the other hand, incorporation of trivalent ions such as Y^{3+}, B^{3+} and La^{3+} resulted in a decrease in average grain size of HA. In contrary to samples of group 1, there was not a decrease in the grain size of the samples of group 2 including B_2O_3 and La_2O_3 [113].

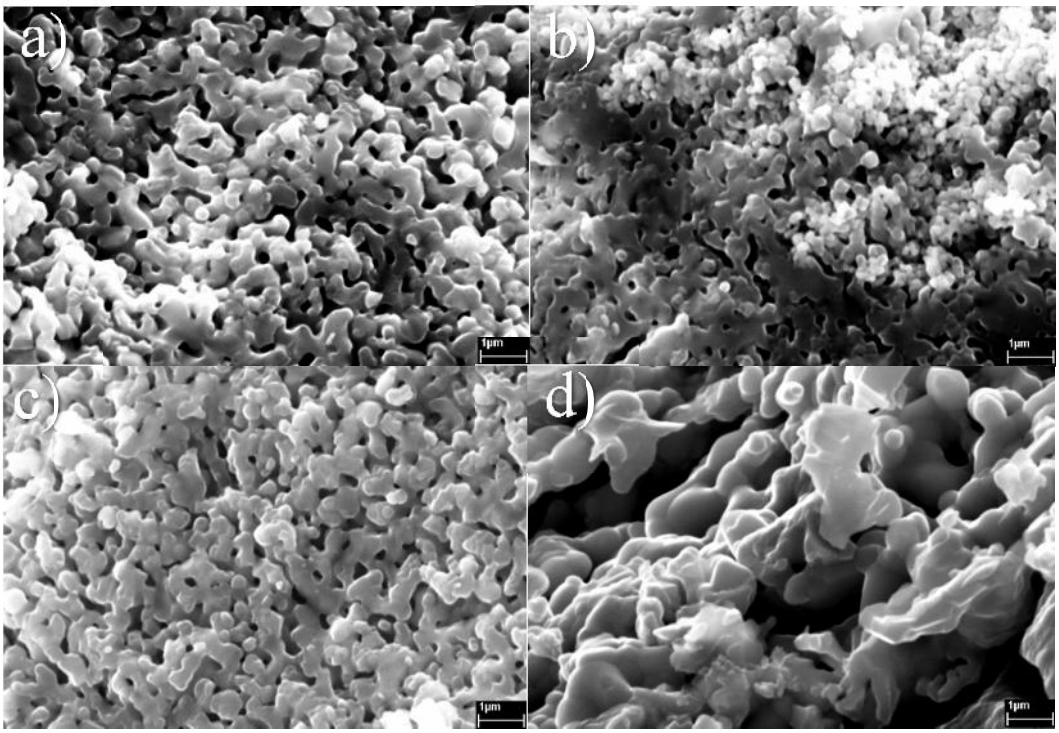

Figure 3.11: SEM images of a) 90HA10B; b) 88HA10B2La; c) 80HA20B; d) 78HA20B2La.

According to Table 3.7, grain size of the composites including ZrO_2 decreased in comparison to that of pure HA. However, composites of group 2 including boron instead of ZrO_2 showed an increase in their average grain size. It was observed that the highest grain size belonged to 78HA20B2La and the lowest belonged to 78HA20Zr2La. It was observed that these results were in perfect correlation with micro-hardness test results. However, there was an unexpected decrease in the average grain size of sample 88HA10B2La. Table 3.7 presents the average grain size values obtained from samples of groups 1 and 2.

Table 3.7: Average grain size for pure HA and different compositions sintered at 1100ºC for 1 h.

Group No	Sample ID	Ave. Grain Size (nm)
1	Pure HA	192
2	90HA10Zr	177
	88HA10Zr2La	173
	80HA20Zr	145
	78HA20Zr2La	115
3	90HA10B	347
	88HA10B2La	296
	80HA20B	363
	78HA20B2La	615

It was reported that there is a direct relationship between the grain size of the apatite and the amount of the dopants in the composition [114]. It was shown that size and growth rate of the grains of the microstructure are different when sintered at different temperatures. It was proven that the grain size of HA is at nano level after being sintered at 900 and 1100ºC, but a high rate of grain growth was observed after being sintered at 1300ºC [114].

It was reported that there was a decrease in the grain size values of HA as the amount of the dopant present in the structure of the composite increased. Also, it was

reported that high sintering temperatures enable HA grains to grow since they provide the required energy to reach the activation energy for growth [114].

3.3 Mechanical Tests

3.3.1 Vickers Micro Hardness Test

Micro-hardness test was conducted to study the effect of different additive materials on the mechanical properties of the composites sintered at 1100ºC for 1h. The resulting values for micro-hardness of the synthesized samples are presented in Table 3.8.

Table 3.8: Micro-hardness values of pure HA and different composite samples sintered at 1100ºC for 1h.

Group ID	Sample ID	Micro-Hardness (GPa)
Group 1	Pure HA	5.13±0.32
	90 HA10Zr	5.54±0.93
	88HA10Zr2La	4.94±0.45
	80HA20Zr	4.04±0.36
	78HA20Zr2La	3.48±0.56
Group 2	90HA10B	2.55±0.21
	88HA10B2La	2.22±0.16
	80HA20B	2.95±0.38
	78HA20B2La	1.85±0.27

The relationship between porosity and the hardness was studied and it was reported that hardness and porosity have an opposite relationship as an increase in hardness requires a decrease in the porosity of the structure, which is known as the Duckworth-knudsen exponential model [115].

It was observed that addition of ZrO_2 to the HA composite enhanced the micro-hardness of the sample but an increase in the amount of ZrO_2 content in composite led to a decreasing micro-hardness value. Introducing La_2O_3 into the composite of HA and ZrO_2 was also studied and it was concluded that the addition of La_2O_3 also caused the micro-hardness values to decrease.

As obvious in Table 3.8, micro-hardness values of the samples containing only B_2O_3 as additional material decreased as the B_2O_3 content increased. As for the samples containing B_2O_3 and La_2O_3 an increase in the micro-hardness was observed by increasing the content of B_2O_3. It was observed that with the exception of sample 78HA20B2La, composite samples containing B_2O_3 and La_2O_3 showed a decreased level of hardness while hardness values for composite samples containing Zr and La_2O_3 were notably higher.

Among different compositions and materials, sample 90HA10Zr had the highest and sample 88HA10B2La had the lowest hardness values. It was shown that the value of hardness of the samples is in direct linear relationship with the pore content and also can be effected by different factors such as density and grain size so that an increase in either one causes an increase in hardness [116].

3.3.2 Diametral Tensile Strength

In order to measure the tensile strength of the samples, diametral tensile strength test was conducted. Table 3.9 presents diametral strength test results of samples of groups 1 and 2. According to this table, the tensile strength of the composites showed a decrease as the amount of ZrO_2 or La_2O_3 was increased. It was also observed that the tensile strength of the composites including B_2O_3 and La_2O_3 decreased as the introduced amount of each material increased. Also, it was observed that 80HA20Zr and 80HA20B samples had the highest diametral tensile strength values in groups 1 and 2, respectively.

Diametral tensile strength is highly recommended for biomaterials, for example, teeth prosthesis biomaterials and also cement utilize in the dentistry [117]. There is

a great similarity between the stresses formed in implants which are used in dentistry and stresses which are formed during diametral tensile strength test [118]. Previous studies showed that tensile strength values depend on different factors such as porosity, contact area, diameter, thickness, poisson ratio, grain size and distribution of the pores in the samples [118,119]. It was reported that increasing of relative density has a positive effect on diametral tensile strength of HA [120]. Also, presence of second phase has a considerable effect on tensile strength values. Theoretical tensile strength that was reported for completely dense HA is around 35 MPa while for HA which has open pore structure; this value is around 1-2 MPa [121]. This variety in diametral tensile strength values shows that different factors have great effect on test results.

Table 3.9: Diametral tensile strength values of pure HA and different composites. Values in parentheses show standard deviation. 10 samples were used for each measurement.

Group ID	Sample ID	Tensile Strength (MPa)
Group 1	Pure HA	4.12 (0.046)
	90 HA10Zr	6.32 (0.51)
	88HA10Zr2La	6.7 (0.25)
	80HA20Zr	8.32 (1.22)
	78HA20Zr2La	5.15 (1.15)
Group 2	90HA10B	4.86 (1.5)
	88HA10B2La	5.73 (1.27)
	80HA20B	5.91 (1.88)
	78HA20B2La	3.9 (0.89)

It was reported that with a decreasing amount of grain size, mechanical properties of the material were improved. Also, it was reported that presence of a second phase in

the composition resulted in a decrease in mechanical properties of the bio ceramics [122].

3.3.3 Drilling Test

In order to investigate the machinability of the samples, drilling test was performed on pure HA and samples of all different composites. It was observed that except for pure HA and 90HA10Zr sample, all other composite pellets were machinable and did not break during the process. In Figures 3.12-3.13, images of all composite samples and pure HA before and after the drilling test are presented.

Uniform distribution of lanthanum can be one reason for improved machinability. The porosity may also play a role in the optimal machinability as presence of pores could have prevented catastrophic destruction of materials during drilling through crack defection [123].

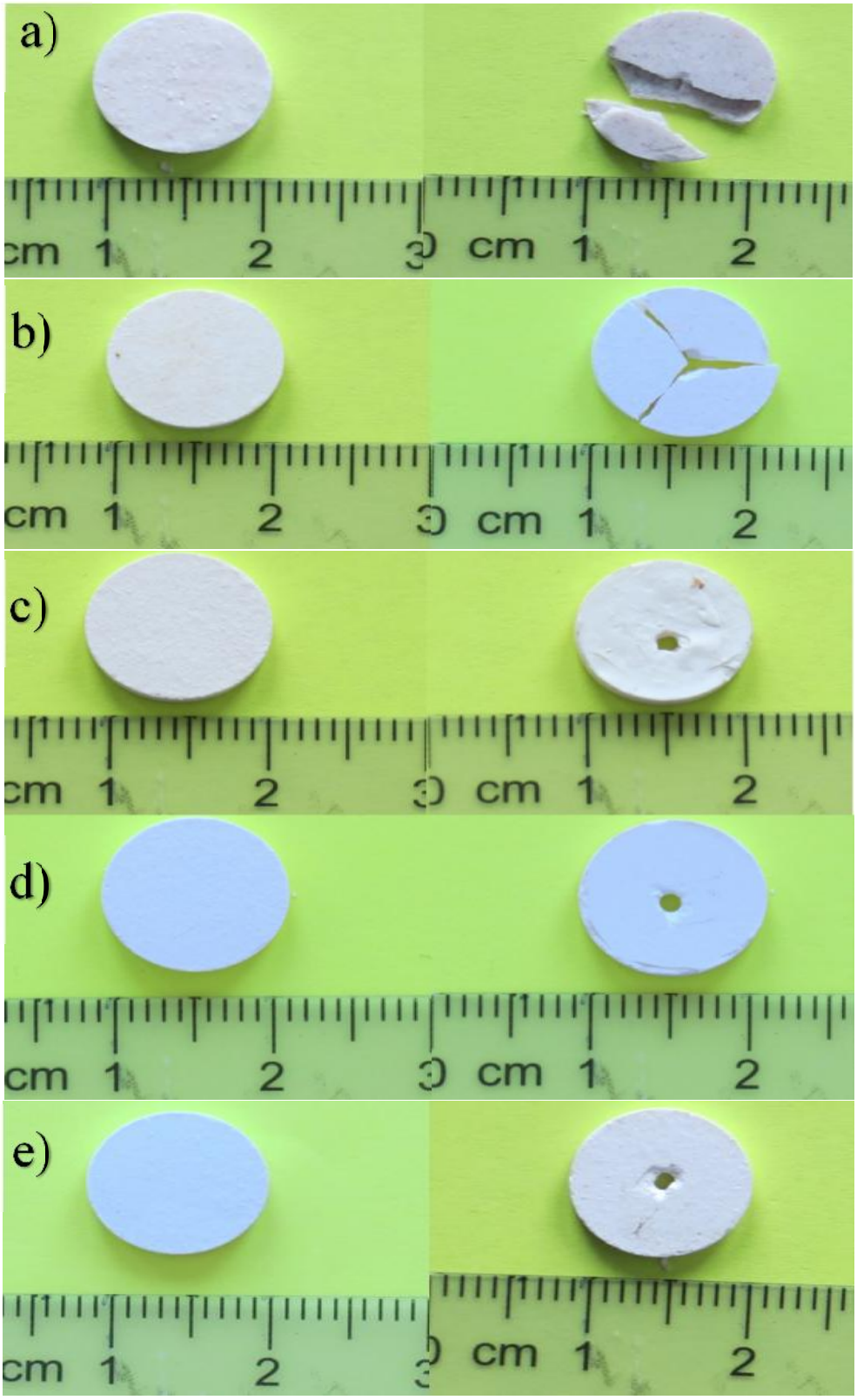

Figure 3.12: Images of drilling test results of a) Pure HA; b) 90HA10Zr; c) 88HA10Zr2La; d) 80HA20Zr; e) 78HA20Zr2La: Before the drilling (left), after the drilling (right).

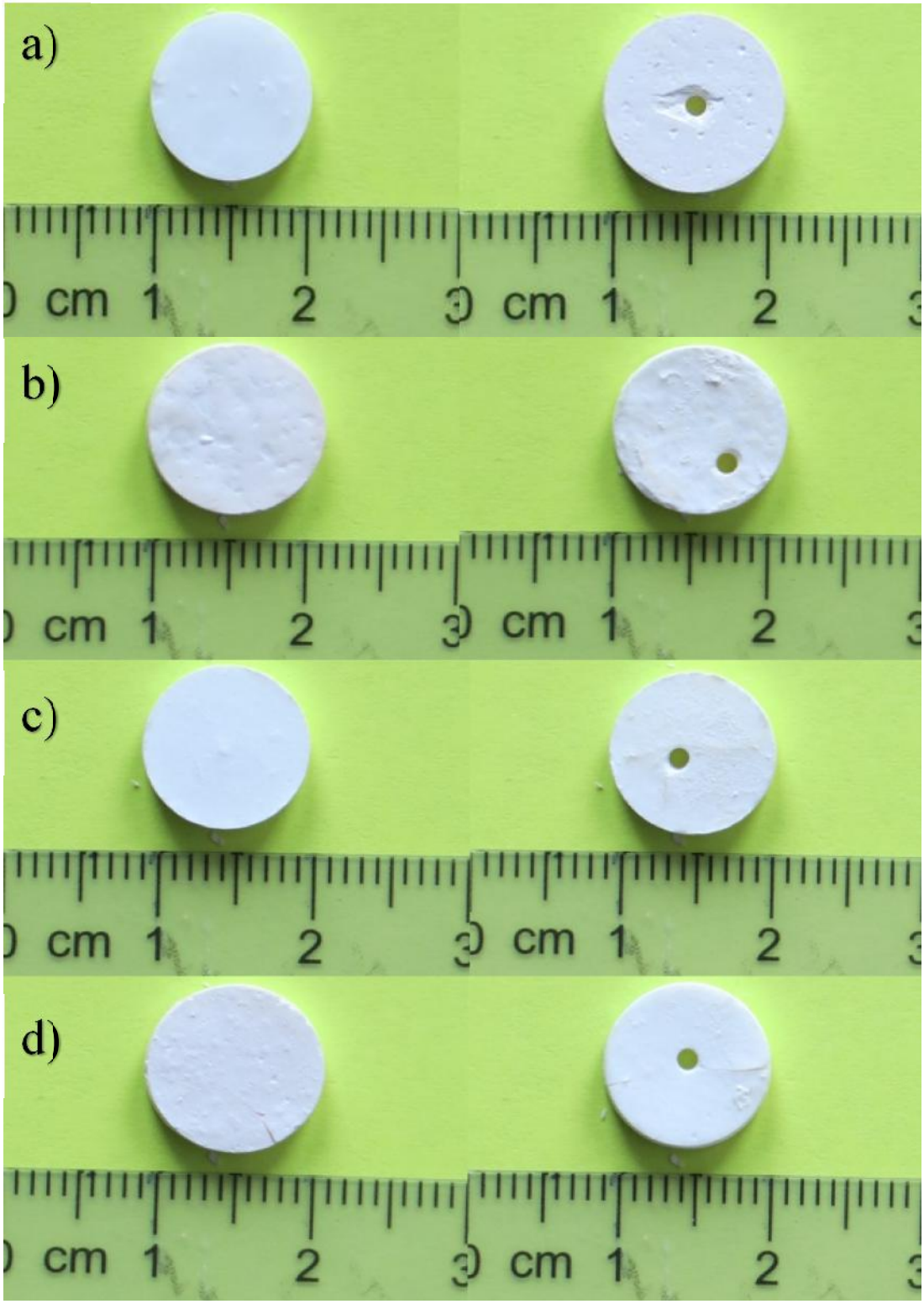

Figure 3.13: Images of drilling test results of a) 90HA10B; b) 88HA10B2La; c) 80HA20B; d) 78HA20B2La: Before the drilling (left), after the drilling (right).

3.4 Biological Characterizations

3.4.1 PrestoBlue™ Assay

Viability of Saos-2 cells on Pure HA and different composites pellets sintered at 1100ºC for 1h was investigated via PrestoBlue™ viability assay which is an indicator of cell proliferation. It was observed that cells seeded on the discs showed perfect attachment from the first day. It was also observed that for the first day, highest cell attachment belongs to pure HA and tissue culture polystyrene (TCPS) samples as expected, while the lowest cell attachment belongs to 90HA10B sample. The reason for the high rate of cell attachment in most of the samples lies within the microstructure of the discs which are porous and also has a direct relationship with grain size of the samples, such that samples with lower grain size showed higher cell attachment rates in comparison to other discs which is also supported repeatedly in literature [124,125,126]. In Figure 3.14 the results of percent reduction of PrestoBlue™ viability reagent are presented. It was also observed that the highest cell viability was observed for TCPS (control) group, then pure HA disc samples among all other composites for at all time points.

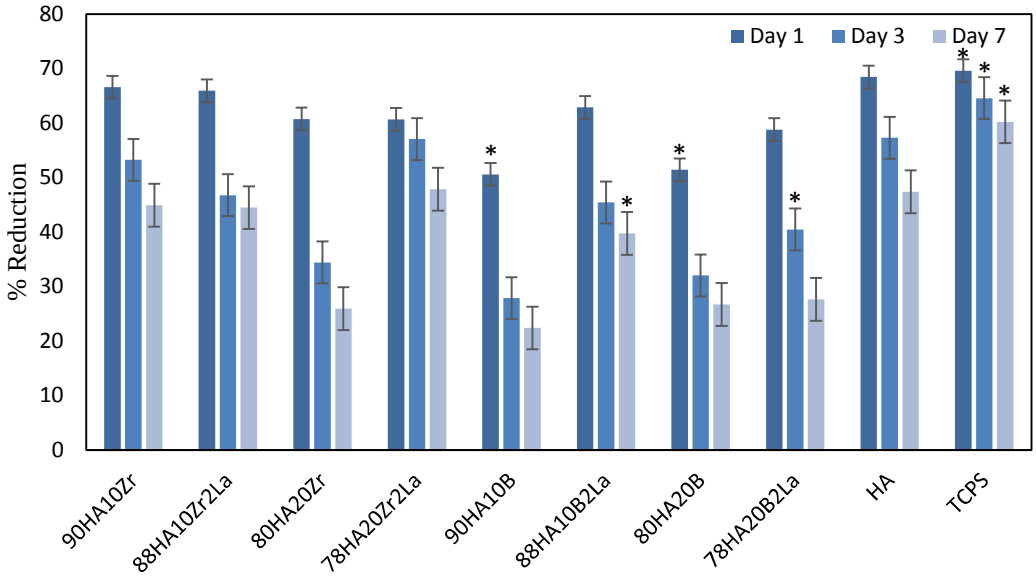

Figure 3.14: Proliferation of cells on pure HA and different composite discs (n=4). Tissue culture polystyrene dish (TCPS) was used as control. The values are depicted as Mean ± SEM.

In this study in samples of group 1, it was observed that increasing amount of ZrO_2 reduced the viability of cells in all groups and all time points which was probably due to degradation in the structure of discs, except for 88HA10Zr2La and 78HA20Zr2La on days 3 and 7. Even though corresponding peaks to such material was not observed in the XRD tests, reduced viability in our samples including ZrO_2 could also be negatively affected by zirconium hydroxide [72].

It was observed that cell viability of all groups decreased with increasing culture time which could be a result of cell confluency on the surface of the discs. This finding was also supported both by SEM images (Figures 3.15-17) and literature [98,127]. Biocompatibility of ZrO_2 was investigated, in vitro, using different cell lines in different biological conditions. Moreover, it was reported that ZrO_2 had little affinity for proteins and cells and that scaffolds containing more than 80% ZrO_2 and lower affinity in compare to others. It was reported that the optimum results are obtained when the amount of ZrO_2 in the material is equal or lesser than 70% of the material [128]. Apart from these, other works suggested that addition of ZrO_2 significantly improved the biocompatibility of the material [128,129,130]. It was reported that viability of cells was negatively affected due to degradation phenomena in the structure of the material [73]. Another study confirmed that ZrO_2 was not cytotoxic, however, some adverse responses were observed which was due to presence of zirconium hydroxide [72].

As for La_2O_3, it was reported that incorporation of La_2O_3 instead of the equivalent Calcium into the apatite has a slightly positive effect on the function of cells. It was also reported that cells with more rich cellular plasma were seen on apatite samples with higher La_2O_3 content. It was confirmed that La_2O_3 at concentrations lower than 1.00×10^{-4} mol l^{-1}, La_2O_3 promoted proliferation, differentiation and function expression of cells but at a higher concentration ($>1.00\times10^{-4}$ mol l^{-1}) it produced obvious damages in microvillus, membranes and endoplasmic reticulum. It was reported that La_2O_3 content lower than 20% has acceptable cytotoxicity [86,123]. In our study, addition of La_2O_3 to the composites increased the viability of cells in all groups and time points except for 88HA10Zr2La in compare to 90HA10Zr at days 1 and 3 which is a probable outcome of ZrO_2 degradation.

Cytotoxicity tests on different cell lines were conducted on different compounds of boron and no cytotoxic responses were reported except for a reduction in cell viability after prolonged exposure (48 h). It was also reported that a moderate reduction in cell viability of about 15% was observed after 18 h at 20 μg/ml [124].

No confirmed range for cytotoxicity of boron has been established yet, however, according to a study, the usual dietary boron consumption is 1-2 mg per day in adult humans [131]. Despite many other works that support positive effect of boron on cell viability, in a recent study, it was reported that incorporation of boron resulted in drastic inhibition of cell proliferation as well as a strong impairment of metabolic activity of the four cell types used [126]. As for samples of group 2, it was proved that increasing amount of B_2O_3 increased the viability of cells in 90HA10B and 80HA20B samples for all time points. Also, incorporation of La_2O_3 improved cell viability in both 88HA10B2La and 78HA20B2La. However, increasing amount of B_2O_3 in presence of La_2O_3, resulted in an opposite effect and reduced the viability for 78HA20B2La in comparison to 88HA10B2La.

No study was found regarding the investigation of the biocompatibility of the composites of HA, ZrO_2/B_2O_3 and La_2O_3.

It was also observed that samples of group 1 containing ZrO_2 illustrate higher viability in comparison to those of group 2 containing B_2O_3 with the exception of 80HA20Zr and 80HA20B on day 7 which sample 80HA20B has a slightly higher viability. It was observed that samples 90HA10B, 80HA20B and TCPS hold the highest number of data among other groups for day 1.

It was observed that 90HA10B, 80HA20B and TCPS samples had a statistically higher cell attachment from other groups such that TCPS held the highest as expected and supported by literature and 90HA10B and 80HA20B held the lowest cell viability rates which has most probably as a result of partial confluency of cells on discs. As for the results of day 3 and day 7, it was observed that cell viability value for all the groups had high statistical significant. It was observed that the cell viability on 90HA10B was significantly higher than other discs and that TCPS held the highest cell viability values as expected. As for results of day 7, it was observed

that 88HA10B2La had significantly higher cell number than other cell groups. Additionally, the viability of cells observed for this group was comparable to both TCPS and HA groups.

The complete analysis report of Tukey's multiple Comparisons test and 1 way ANOVA test are presented in Appendix A and B, respectively.

3.4.2 Scanning Electron Microscopy

The morphology of cells on pure HA and different composite discs were examined by SEM analysis (Figures 3.15-3.17) after 1 and 7 days of incubation. Cells attached and covered almost the entire surface of discs, forming layers of cell sheet starting from day 1. After 1 day of incubation the cells spread on the surface of the discs. Complete coverage indicated that surface properties were ideal for cell attachment and spreading.

It was reported that pores and tiny cracks make specific surface area larger and easier to bond with surrounding tissue in vivo, thus providing brackets and passages for the growth of the new bone tissue, hence the better biocompatibility [132]. In another study, it was reported that cell division and proliferation is known to be a coordinated process ruled by cell-cell signaling. Once the cell-layer on a substrate becomes confluent, the cell signaling for the proliferation gets restricted, causing cellular division and proliferation to stop. Also in some SEM images, cell filopodias were broken which was reported to be a result of drying out during the fixation process, or is a sign of a necrotic cell [133].

In our study, it was observed that pure HA disc samples (Figure 3.16-c) had the highest surface coverage with cells, both in days 1 and 7 which was in agreement with our cell viability results. The fact that cells covered the entire surface of discs from day 1 could be due to high initial cell seeding density. After 7 days of incubation, both cuboidal and dendritic shaped cell clusters were observed in scattered patterns over the disc surface. This was due to lack of attachable surface for proliferated cells (Figure 3.17-c) which in turn caused viability of cells to reduce

with culture time. Cell sheet coverage was observed at the end of day 7 in the periphery of discs and also inside the cracks and grooves of the surface. Also, it was observed that at the end of day 7 thick layers of cell sheets have covered the surface of the discs which resulted in reduced viability readings since the cell layers underneath others did not have access to culture medium (Figures 3.16-c and 3.17-a) which was in agreement with cell viability results. It was observed that samples 90HA10Zr and 88HA10B2La (Figures 3.16-a and 3.17-f) had the highest value of cell viability at the end of day 1 among composites of group 1 and 2, respectively. As for samples of day 7, it was observed that 78HA20Zr2La and 80HA20B (Figures 3.17-a and 3.17-d) had the highest cell viability among composites of groups 1 and 2, respectively.

Due to confluency on most of the samples the structure of the surface was not visible. SEM image for 80HA20B sample had a thin layer of cell sheet spread all over, which was distinguishable as an opaque layer covering small grains.

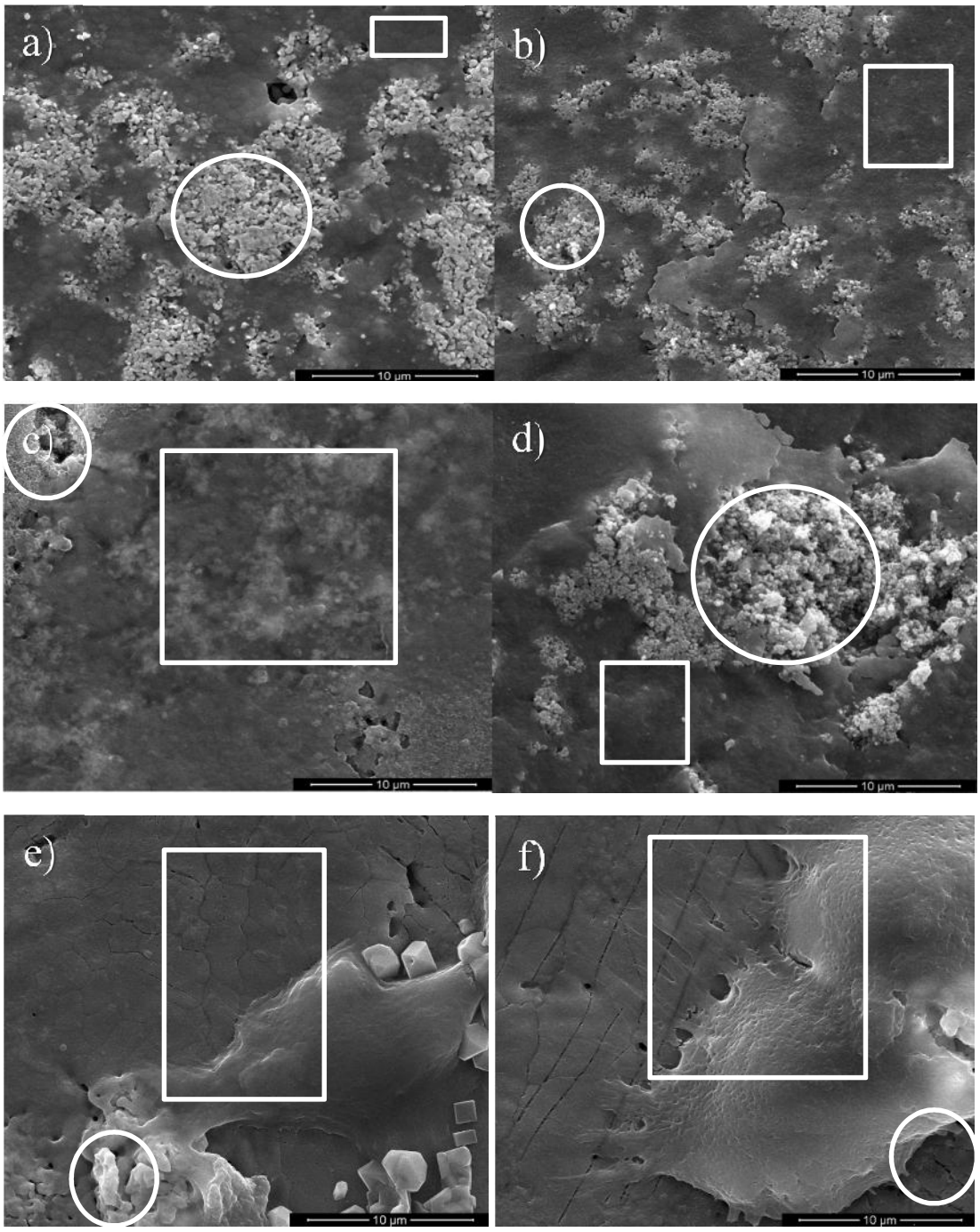

Figure 3.15: SEM images of cells seeded on a) 90HA10Zr; b) 88HA10Zr2La; c) 80HA20Zr; d) 78HA20Zr2La; e) 90HA10B; f) 88HA10B2La; discs after 1 day of incubation at 37ºC in a carbon dioxide incubator. Rectangles represent cell sheet and circles represent material surface.

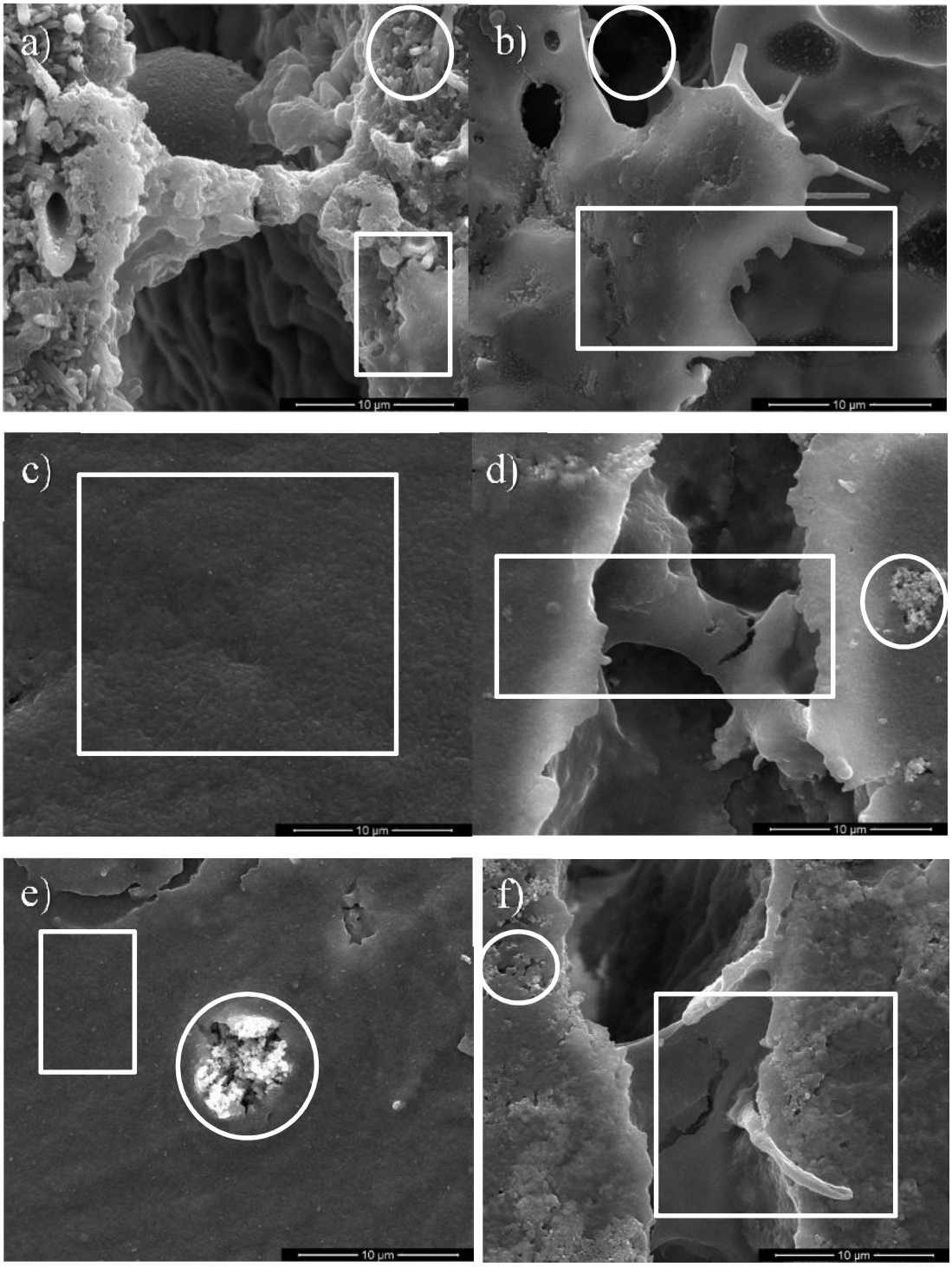

Figure 3.16: SEM images of cells seeded on a) 80HA20B; b) 78HA20B2La; c) pure HA after 1 day and d) 90HA10Zr; e) 88HA10Zr2La; f) 80HA20Zr; discs after 1 day of incubation at 37ºC in a carbon dioxide incubator. Rectangles represent cell sheet and circles represent material surface.

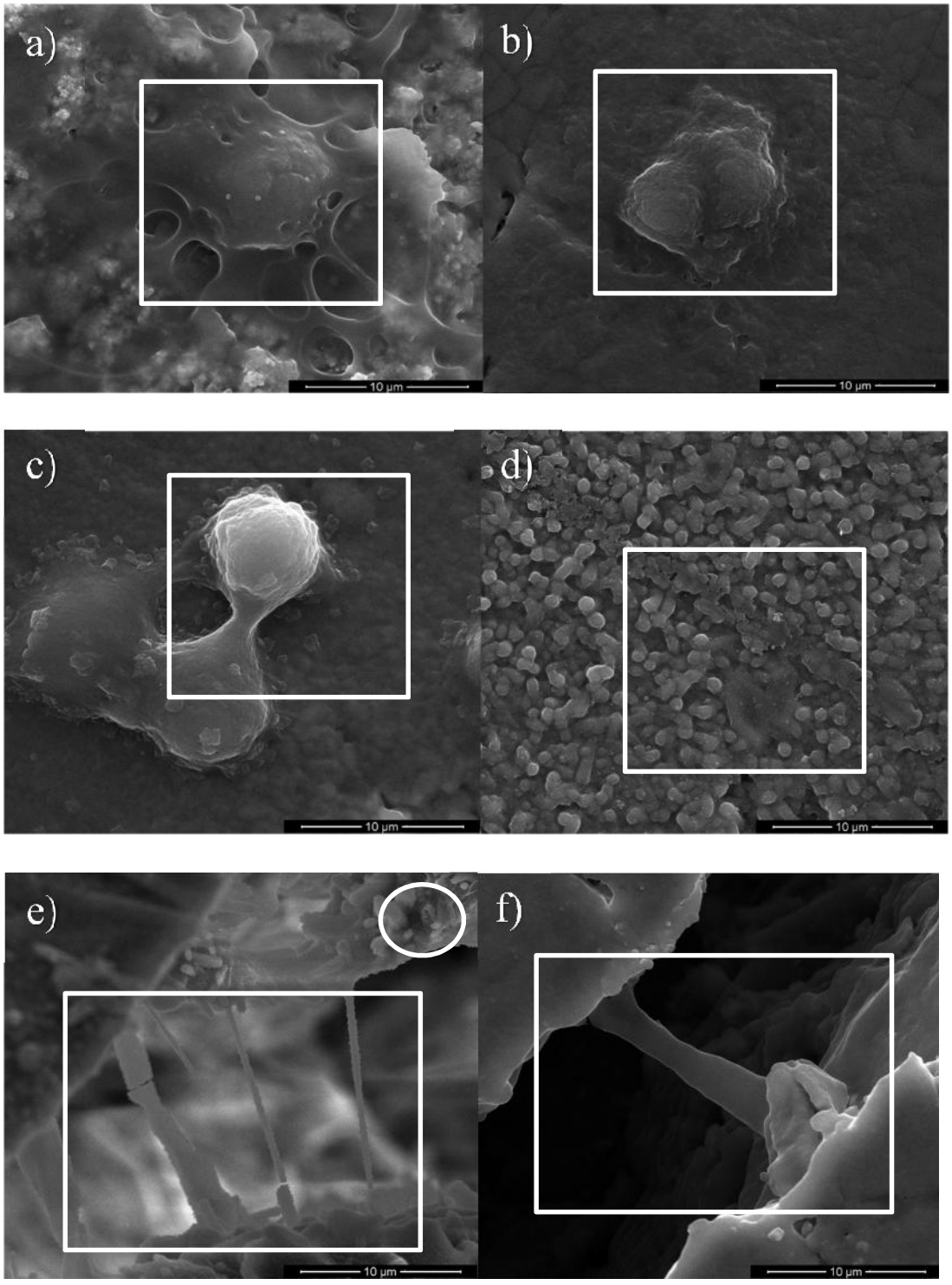

Figure 3.17: SEM images of cells seeded on a) 78HA20Zr2La; b) 90HA10B; c) 88HA10B2La; d) 80HA20B; e) 78HA20B2La; f) pure HA discs after 1 day of incubation at 37ºC in a carbon dioxide incubator. Rectangles represent cell sheet and circles represent material surface.

CHAPTER 4

CONCLUSIONS

In this study HA was synthesized by precipitation method and then mixed in different amounts, with ZrO_2, B_2O_3 and La_2O_3 in order to investigate its microstructure and mechanical properties. Composite samples were sintered at 1100ºC for 1h.

Density of the composites including ZrO_2 and La_2O_3 increased in all of compositions except for sample 78HA20Zr2La. On the contrary, densities of all the samples including B_2O_3 and La_2O_3 decreased in comparison to that of HA.

Presence and weight percentage of different atoms present in the structure of the composites were investigated via EDX. It was observed that addition of ZrO_2 or introduction of La_2O_3 results in increasing Ca/P ratio in the composites. No peaks corresponding to boron was observed since boron is a light element and cannot be identified via EDX. Composites including B_2O_3 or La_2O_3 behaved differently and did not follow a pattern.

Mercury intrusion porosimetry was conducted on composites to determine their percent porosity. It was observed that addition of ZrO_2 or B_2O_3 or introduction of La_2O_3 resulted in an increased porosity for samples.

Presence of different phases and existence of different chemical bonds were confirmed via XRD and FTIR tests. It was seen that presence of ZrO_2 and B_2O_3 in the structure of the composites increased the rate of HA decomposition, except for

sample 78HA20B2La which revealed a notable decrease in the intensity of its peaks. Trace amounts of β-TCP were seen in the structure of the composite.

Scanning electron microscopy (SEM) results proved that addition of ZrO_2 and La_2O_3 to the composite resulted in smaller grain size. On the other hand, in composites including B_2O_3 and La_2O_3, grain size was increased noticeably, especially for 78HA20B2La sample, which was in correlation with other obtained results.

Vickers's micro-hardness and diametral tests were performed on the samples and it was seen that addition of ZrO_2 to the composite enhanced mechanical properties of the composite in certain compositions. However, composites with B_2O_3 did not experience the same results and their micro-hardness values decreased.

In order to investigate the machinability of the composite discs, drilling tests were conducted and it was proved that except for sample 90HA10Zr and pure HA, all of the samples are machinable and did not break during the experiment.

The viability and morphology of Saos-2 cells on HA and composites were investigated in cell culture studies. PrestoBlue™ assay results revealed that cells attached and spread on all disc groups after 1 day of incubation. It was concluded that composites including ZrO_2 in their structure have a better attachment starting from day 1 compared to composites including B_2O_3. Also it was observed that highest cell attachment and proliferation were observed on TCPS followed by pure HA. The viability of cells decreased with culture time because, as also confirmed by SEM images, cell sheets covered almost the entire surface of discs. SEM images proved the confluency of cells starting from day 1 and showed good attachment of cells to surface. Also, it was observed that cell sheets covered the inside surface of grooves and cracks in the structure of the samples, proving that all materials used in this study, considering the dose range, are biocompatible and suitable for use as an implant.

There are also some areas that needs further development and can probably improve the results obtained in this thesis. The sintering method used in this study to obtain the discs was air sintering which might not be the best method, since composites

have shown better mechanical and biological results in hot isostatic sintering and pressure sintering. Also in case of biological tests and to evaluate the differentiation of the cells, alkaline phosphatase activity and dissolution tests can be conducted.

REFERENCES

[1] A. R. Gazdag, J. M. Lane, D. Glaser, R. A. Foster, "Alternatives to autogenous bone graft: efficacy and indications", Journal of the American Academy of Orthopedic Surgeons, vol. 3, (1995) 1-8.

[2] P. X. Ma, R. Zhang, G. Xiao, R. Fanceschi, "Engineering new bone tissue in vitro on highly porous poly(alpha-hydroxyl acids)/ hydroxyapatite composite scaffolds", Journal of Biomedical Material Research, vol. 54, (2001) 284-293.

[3] D. C. Dunand, "Processing of titanium foams", Advanced Engineering Materials, vol. 6, (2004) 369-376.

[4] N. Kotobuki, K. Loku, D. Kawagoe, H. Fujimori, S. Goto, H. Ohgushi, "Observations of osteogenic differentiation cascade of living mesenchymal stem cells on transparent hydroxyapatite ceramics", Biomaterials , vol. 26, (2005) 779-785.

[5] E. J. Lee, Y. H. Koh, B. H. Yoon, H. E. Kim, H. W. Kim, "Highly porous hydroxyapatite bio ceramics with interconnected pore channels using camphene-based freez-cating", Materials Letters , vol. 61, (2007) 2270-2273.

[6] I. H. Jo, K. H. Shin, Y. M. Soon, J. H. Lee, H. E. Kim, "Highly porous hydroxyapatite scaffolds with elongated pores using stretched polymeric sponges as novel template", Materials Letters , vol. 63, (2007) 1702-1704.

[7] L. Mosekilde, "Normal vertebral body size and compressive strength: relations to age and to vertebral and iliac trabecular bone compressive strength", Bone, vol. 7, (1986) 207-212.

[8] J. L. Masonis, R. B. Bourne, M. D. Ries, R. W. McCalden, A. Salehi, D. C. Kelman, "Zirconia femoral head fractures: a clinical and retrieval analysis", Journal of Arthoplasty , vol. 19, (2004) 898-905.

[9] J.C. Elliott, R.M. Wilson, S. Dowker, "Apatite Structure", Advances in X-ray Analysis, vol. 45, (2002) 172-181.

[10] D. McConnell, "Apatite: Its crystal chemistry, mineralogy, utilizat ion, and geologic and biologic occurrences", Springer-Verlag, 12 (1973) 1-63.

[11] J. Elliott, "Structure and chemistry of the apatites and other calcium orthophosphates", Elsevier, (1994) 4-62.

[12] S. Weiner, HD. Wagner, "The Material Bone: Structure-Mechanical Function Relations", Annual Review Materials Science, vol. 28, (1998) 271-298.

[13] F.H. Martini, J.L. Nath, in Fundamentals of Anatomy and Physiology, (2009) 185-193.

[14] C. Cowin, in Bone Mechanics, CRC Press, (1989) 97-157.

[15] P. Gehron-Robey, A.L. Boskey, in the Biochemistry of Bone, London, UK, Academic Press, (1996) 90-120.

[16] G. Herring, "The Organic Matrix of Bone" in the Biochemistry and Physiology of Bone, NY, USA, Academic Press, (1972) 127-189.

[17] B. Hall, in Bone matrix and bone specific products, Boca Raton, USA, CRC Press, (1991) 55-70.

[18] R.B. Martin, D.B.Burr, in Structure, function, and adaptation of compact bone, NY, USA, Raven Press, (1989) 34-230.

[19] R. Lakes, "Materials with structural hierarchy", Nature, 361, (1993) 511-515.

[20] W. Jee, "Structure and function of bone tissue, in orthopedics, Principles of basic and clinical science", Boca Raton, USA, CRC Press, (1999) 112-238.

[21] R.B. Martin, D.B. Burr, N.A. Sharkey, in Skeletal Tissue Mechanics, NY, USA, Springer, (1998) 29-80.

[22] J. Currey, Bones: Structure and Mechanics, Princeton University Press, (2002) 54-173.

[23] D.M. Cullinane, T.A. Einhorn, "Biomechanics of bone" in principle of Bone Biology, Second Edition, London, UK, Academic Press, vol. 1, (2002) 17-32.

[24] M.B. Schaffler, D.B. Burr, "Stiffness of compact bone: Effect of porosity and density", Journal of Biomechanics, vol. 21, (1988) 13-16.

[25] S. Weiner, H.D. Wagner, "The material bone: structure mechanical function relations", Annual Review of Materials Science, vol. 28, (1998) 271-298.

[26] J.B. Lian, G.S. Stein, E. Canalis, P. Gehron-Robey, A.L. Boskey, "Bone formation: Osteoblast lineage cells, growth factors, matrix proteins and the

mineralization process", in Prime on the metabolic bone disease and disorders of mineral metabolism, Fourth edition, NY, USA, Academic Press, (1999) 14-29.

[27] N. Sasaki, N. Matsushima, T. Ikawa, H. Yamamura, A. Fukuda, "Orientation of bone mineral and its role in the anisotropic mechanical properties of bone transverse anisotropy", Journal of Biomechanics, vol. 22, (1998) 157-164.

[28] R.B. Martin, D.L. Boardman, "The effect of collagen fiber orientation, porosity, density and mineralization of bovine cortical bone bending properties", Journal of Biomechanics, vol. 26, (1993) 1047-1054.

[29] W. Whitehouse, "The quantitative morphology of anisotropic trabecular bone", Journal of Microscopy, vol. 101, (1974) 153-168.

[30] V.H. Frankel, M. Nordin, in Basic Biomechanics of Skeletal System, Philadelphia, PA, USA, Lea & Febiger, (1980) 22.

[31] A. L. Kierzenbaum, Histology and Cell Biology. An Introduction to Pathology, St. Louis, MO, USA, Mosby Inc., (2002).

[32] A. Boskey, "Bone mineral crystal", Osteoporosis International, 14, (2003) 16-21.

[33] W. Kossler, J. Fuchs, "Calcium orthophosphates as biomaterials and bio ceramics" in S.V. Dorozhkin "Bio ceramics, properties, preparation and applications", Nova Science Publishers, (2009) 65-159.

[34] S.M. Besta, A.E. Porter, E.S. Thian, J. Huang, "Bio ceramics: Past, present and for the future", Journal of the European Ceramic Society, vol. 28, (2008) 1319–1327.

[35] R.K. Rude, "Magnesium homeostasis" in J.P. Bilezikian, L.G. Raisz, G.A. Rodan (Ed.), Principles of Bone Biology, Academic Press 1, (2002) 339-358.

[36] A. Bigi, G. Falini, E. Foresti, M. Gazzano, A. Ripamonti, N. Roveri, "Magnesium influence on hydroxyapatite crystallization", Journal of Inorganic Biochemistry, vol. 49, (1993) 69-78.

[37] R. LeGeros, "Calcium phosphates in oral biology and medicine", in Monographs in Oral Science, ed. K.H. Myers, Basel, Switzerland, AG Publishers, (1991) 82-107.

[38] Z. Evis, "Reactions in hydroxyapatite-zirconia composites", Ceramics International, vol. 33, (2007) 987-991.

[39] F. Bronner, "Metals in bone" in J.P. Bilezikian, L.G. Raisz, G.A. Rodan (Ed.), Principles of Bone Biology, Academic Press 1, (2002) 359-369.

[40] W.G. Goodman, M.E. Duarte, "Aluminum: effects on bone and role in the pathogenesis of renal osteodystrophy", Mineral and Electrolyte Metabolism, vol. 17, (1991) 221-232.

[41] P.C. D'Haese, M.M. Coutteney, M.E. De Broe, "Diagnosis and treatment of aluminum bone disease", Nephrology, Dialysis and Transplantation, vol. 11, (1996) (Suppl. 3) 74-79.

[42] T. Miyahara, H. Yamada, M. Takeuchi, H. Kozuka, T. Kato, H. Sudo, "Inhibitory effects of cadmium on in vitro calcification of a clonal osteogenic cell", Toxicology and Applied Pharmacology , vol. 96, (1998) 52-59.

[43] Y. Hojima, B. Behta, A.M. Romanic, D.J. Prockop, "Cadmium ions inhibit procollagen C-proteinase and cupric ions inhibit procollagen N-proteinase", Journal of International Society for Matrix Biology, vol. 14, (1994) 113-120.

[44] S.G. Dahl, P. Allain, P.J. Marie, Y. Mauras, G. Boivin, P. Ammann, Y. Tsoderous, P.D. Delmas, C. Christiansen, "Incorporation and distribution of strontium in bone", Bone, vol. 28, (2010) 446-453.

[45] V. Persy, G. Behets, A. Bervoets, M. De Broe, P. D'Haese, "Lanthanum: a safe phosphate binder," Seminars in Dialysis, vol. 19, (2006) 195-199.

[46] E. Jallot, J.M. Nedelec, A.S. Grimault, E. Chassot, "STEM and EDXS characterization of physic-chemical reaction at the periphery of sol-gel derived Zn-substituted hydroxyapatites during interaction with biological fluids", Colloids and Surfaces B: Bio interfaces, vol. 42, (2005) 205-210.

[47] P. Van Landuyt, F. Li, J.P. Keustermans, J.M. Streydio, F. Delannay, E. Munting, "The influence of high sintering temperatures on the mechanical properties of hydroxyapatite", Journal of Materials Science: Materials in Medicine, vol. 6, (1995) 8-13.

[48] S. S. Kulkarni, Y. Yong, M.J. Rys, S. Lei, "Machining assessment of nano-crystalline hydroxyapatite", Journal of Manufacturing Processes, vol. 15, (2013) 666-672.

[49] R. Z. Legeros, J. P. Legeros, in L. L. Hench, J. Wilson, editors, “An Introduction to Bio ceramics”, Singapore, World Scientific Publishing Company, (1993) 139-180.

[50] S. A. Guechler, J. O. Holinger, "An Introduction to Biomaterials", Boca Raton, USA, CRC Press, (2006) 311-339.

[51] G. Ma, X. Y. Liu, "Hydroxyapatite: Hexagonal or monoclinic?” Crystal Growth and Design, vol. 9, (2009) 2991-2994.

[52] Q. Song, C. Wang, S. Wen, "Effects of doping on crystal and grain boundary in human enamel", Materials Science and Engineering A, vol. 297, (2001) 272-280.

[53] S. Pramanik, A. K. Agarwal, K. N. Rai, A. Garg, "Development of high strength hydroxyapatite by solid-state-sintering process", Ceramics International, vol. 33, (2007) 419-426.

[54] S. H. Rhee, "Synthesis of hydroxyapatite via mechanochemical treatment", Biomaterials, vol. 23, (2002) 1147–1152.

[55] W. Feng, L. Mu-sen, L. Yu-peng, Q. Yong-xin, "A simple sol–gel technique for preparing hydroxyapatite nanopowders", Materials Letters, vol. 59, (2005) p. 916– 919.

[56] K. P. Sanosh, M. C. Chu, A. Balakrishnan, T. N. Kim, S.J. Cho, "Sol-gel synthesis of pure nanosize β-tricalcium phosphate crystalline powders", Current Applied Physics, vol. 10, (2010) 68-71.

[57] I. Mobasherpour, M. S. Heshajin, A. Kazemzadeh, M. Zakeri, "Synthesis of nanocrystalline hydroxyapatite by using precipitation method", Journal of Alloys and Compounds, vol. 430, (2007) 330-333.

[58] W. J. Shih, Y.H. Chen, M. C. Wang, M. H. Hon, "Crystal growth and morphology of the nano-sized hydroxyapatite powders synthesized from $CaHPO_4*2H_2O$ and $CaCO_3$ by hydrolysis method", Journal of Crystal Growth, vol. 270, (2004) 211-218.

[59] V. P. Orlovskii, V. S. Komlev, S. M. Barinov, "Hydroxyapatite and hydroxyapatite-based ceramics," Inorganic Materials, vol. 38, (2002) 1159-1172.

[60] Z. Evis, R. H. Doremus, "Coatings of hydroxyapatite-nanosize alpha alumina composites on Ti-6Al-4V," Materials Letters, vol. 59, (2005) 3824-3827.

[61] S. Ramesh, C. Y. Tan, I. Sopyan, M. Hamdi, W. D. Teng, "Consolidation of nanocrystalline hydroxyapatite powder", Science and Technology of Advanced Materials, vol. 8, (2007) 124-130.

[62] M. A. Meyers, P. Y. Chen, A. Y. M. Lin, Y. Seki, "Biological materials: Structure and mechanical properties", Progress in Materials Science, vol. 53, (2008) 1-206.

[63] L.-H. He, O. C. Standard, T. T. Y. Huang, B. A. Latella, M. V. Swain, "Mechanical behavior of porous hydroxyapatite", Acta Biomaterialia, vol. 4, (2008) 577-586.

[64] J. J. Klawitter, S. F. Hulbert, "Application of porous ceramics for the attachment of load bearing internal orthopedic applications", Journal of Biomedical Materials Research, vol. 5, (1971) 161-229.

[65] R. A. Ayers, L. M. Wolford, T. A. Bateman, V. L. Ferguson, S. J. Simske, "Qualification of bone ingrowth into porous block hydroxyapatite in humans", Journal of Biomedical Materials Research, vol. 47, (1999) 54-59.

[66] H. Denissen, C. Mangano, G. Venini, "Hydroxyapatite implants", Piccin Nuova Libraria, Spa: Padua , (1985) 160-170.

[67] T. Kokubo, "Bio ceramics and their clinical applications", Boca Raton, USA, CRC Press, (2008) 92-353.

[68] A. Zamiri, S. De, "Mechanical properties of hydroxyapatite single crystals from nanoindentation data", Journal of the Mechanical Behavior of Biomedical Materials, vol. 4, (2011) 146–152.

[69] A. Ito, K. Teraoka, S. Tsutsumi, T. Tateishi, "Single crystal hydroxyapatite: Preparation, composition and mechanical properties", in T. Kokubo, T. Nakamura, F. Miyaji, Bio ceramics, Pergamon Press, (1996) 189-192.

[70] E. Fernândez, F.J. Gil, M.P. Ginebra, F.C.M. Driessens, J.A. Planell, S.M. Best, "Calcium phosphate bone cements for clinical applications. Part I: Solution chemistry", Journal of Materials Science: Materials in Medicine, vol. 10, (1999) 169-176.

[71] W. Chen, S. Oh, A.P. Ong, N. Oh, Y. Liu, H.S. Courtney, M. Appleford, J.L. Ong, "Antibacterial and osteogenic properties of silver-containing hydroxyapatite coatings produced using a sol gel process", Journal of Biomedical Materials Research Part A, vol. 82A, (2007) 899-906.

[72] P. F. Manicone, P. R. Iommetti, L. Raffaelli, "An overview of zirconia ceramics: Basic properties and clinical applications", Journal of Dentistry, vol. 35, (2007) 819-826.

[73] C. Piconi, G. Maccauro, "Zirconia as a ceramic biomaterial", Biomaterials, vol. 20, (1999) 1-25.

[74] X. Miao, Y. Hu, J. Liu, X. Huang, "Hydroxyapatite coating on porous zirconia", Materials Science and Engineering C, vol. 27, (2007) 257-261.

[75] S.H. Ana, T. Matsumoto, H. Miyajimaa, A. Nakahirab, "Porous zirconia/hydroxyapatite scaffolds for bone", Dental Materials, vol. 28, (2012) 1221-1231.

[76] Z. Evis, M. Usta, I. Kutbay, "Improvement in sinterability and phase stability of hydroxyapatite and partially stabilized zirconia composites", Journal of the European Ceramic Society, vol. 29, (2009) 621-628.

[77] A. Rapacz-Kmitaa, A. S. Losarczyka, Z. Paszkiewicza, C. Paluszkiewicz, “Phase stability of hydroxyapatite-zirconia (Hap-ZrO2) composites for bone replacement”, Journal of Molecular Structure, vol. 704, (2004) 333-340.

[78] J. Tinschert, G. Natt, W. Mautsch, M. Augthun, H. Spiekermann, "Fracture resistance of lithium disilicate-, alumina-, and zirconia based three-unit fixed partial dentures: a laboratory study", International Journal of Prosthodontic, vol. 14, (2001) 231-238.

[79] W. Att, M. Grigoriadou, JR. Strub, "ZrO2 three-unit fixed partial dentures: comparison of failure load before and after exposure to a mastication simulator", Journal of Oral Rehabilitation, vol. 34, (2007) 282-290.

[80] J. Swab, “Low temperature degradation of Y-TZP materials", Journal of Materials Science, vol. 26, (1991) 6706-6714.

[81] L. Sennerby, A. Dasmah, B. Larsson, M. Iverhed, "Bone tissue responses to surface-modified zirconia implants: A histomorphometric and removal torque

study in the rabbit", Clinical Implant Dentistry and Related Research, vol. 7, (2005) S13-S20.

[82] L. Rimondini, L. Cerroni, A. Carrassi, P. Torricelli, "Bacterial colonization of zirconia ceramic surfaces: an in vitro and in vivo study", International Journal of Oral Maxillofacial Implants, vol. 17, (2002) 793-798.

[83] RJ. Kohal, G. Klaus, JR. Strub, "Zirconia-implant-supported all ceramic crowns withstand long-term load: a pilot investigation", Clinical Oral Implants Research, vol. 17, (2006) 565-571.

[84] E. Yoshikawa, A. Sasaki, M. Endo, "Removal of boron from wastewater by the hydroxyapatite formation reaction using acceleration effect of ammonia", Journal of Hazardous Materials, vol. 237-238, (2012) 277-282.

[85] D. Lahiri, V. Singh, A.P. Benaduce, S. Seal, L. Kos, A. Agarwal, "Boron nitride nanotube reinforced hydroxyapatite composite: Mechanical and tribological performance and in-vitro biocompatibility to osteoblasts", Journal of the Mechanical Behavior of Biomedical Materials, vol. 4 (2011) 44-56.

[86] D.G. Guo, A.H. Wang, Y. Han, K.W. Xu, "Characterization, physiochemical properties and biocompatibility of La-incorporated apatites," Acta Biomaterialia, vol. 5, (2009) 3512-3523.

[87] C. Ergun, "Synthesis and characterization of machinable calcium phosphate/lanthanum phosphate composites", Journal of Materials Processing Technology, vol. 199, (2008) 178-184.

[88] ASTM, "Standard Test Methods for Determining Average Grain Size," ASTM, Pennsylvania, United states, (2014).

[89] G.F. Kamst, J. Vasseur, C. Bonazzi, J.J. Bimbenet, "A new method for the measurement of the tensile strength of rice grains by using the diametral compression test", Journal of Food Engineering, vol. 40, (1999) 227-232.

[90] J. Jang, S. Kim, "Factors affecting diametral tensile strength of microfilled dental composites", Polymer Journal, vol. 28, (1996) 293-298.

[91] Z. Evis, C. Ergun, R.H. Doremus, "Hydroxylapatite-zirconia composites: Thermal stability of phases and sinterability as related to the CaO-ZrO2 phase diagram", Journal of Materials Science, vol. 40, (2005) 1127-1134.

[92] D. Lahiri, F. Rouzaud, T. Richard, A.K. Keshri, S.R. Bakshi, "Boron nitride nanotube reinforced polylactide–polycaprolactone copolymer composite: Mechanical properties and cytocompatibility with osteoblasts and macrophages in vitro", Acta Biomaterialia, vol. 6, (2010) 3524–3533.

[93] G. Ciofani, S. Danti, S. Nitti, B. Mazzolai, V. Mattoli, M. Giorgi, "Biocompatibility of boron nitride nanotubes: An up-date of in vivo toxicological investigation", International Journal of Pharmaceutics, vol. 444, (2013) 85-88.

[94] C. Zhi, Y. Bando, C. Tang, D. Golberg, "Boron nitride nanotubes", Materials Science and Engineering R, vol. 70, (2010) 92-111.

[95] F.N. Oktar, S. Ozyegin, O. Meydanoglu, H. Aydin, S. Agathopoulos, G. Rocha, B. Sennaroglu, S. Kayali, "Sintering effect on mechanical properties of composites of Hydroxyapatite Lanthanum Oxide (HA-La2O3)", Key Engineering Materials , Vols. 309-311, (2006) 101-104.

[96] M. Descamps, J.C. Hornez, A. Lerich, "Effect of powders stoichiometry on the sintering of β-tricalcium phosphate", Journal of the European Ceramic Society, vol. 27, (2007) 2401-2406.

[97] R.B. Heimann, T.A. Vu, "Effect of CaO on thermal decomposition during sintering of composite hydroxyapatite–zirconia mixtures for monolithic ceramic implants", Journal of Materials Science Letters, vol. 16, (1997) 437-439.

[98] C. Ergun, H. Liu, T.J. Webster, "Osteoblast adhesion on novel machinable calcium phosphate/lanthanum phosphate composites for orthopedic applications", Journal of Biomedical Materials Research A, vol. 89(3), (2009) 727-733.

[99] R. Murugan, S. Ramakrishna, "Effect of zirconia on the formation of calcium phosphate bioceramics under microwave irradiation", Materials Letters, vol. 58, (2003) 230-234.

[100] A. Slosarczyk, C. Paluszkiewicz, M. Gawlicki, Z. Paszkiewicz, " The FTIR spectroscopy and QXRD studies of calcium phosphate based materials produced from the powder precursors with different Ca/P ratios", Ceramics International, vol. 23, (1997) 297-304.

[101] H. Yang, L. Zhang, K.-W. Xu, "The microstructure and specific properties of La/HAP composite powder and its coating", Applied Surface Science, vol. 254, (2007) 425-430.

[102] R. Ternane, M.Th. Cohen-Adad, G. Pancer, C. Goutaudier, N. Kbir-Ariguib, M. Trabelsi-Ayedi, P. Florian, D. Massiot, "Introduction of boron in hydrxyapatite: synthesis and structural characterization", Journal of Alloys and Compounds, vol. 333, (2002) 62-71.

[103] S. Joschek, B. Nies, R. Krotz, A. Gopferich, "Chemical and physicochemical characterization of porous hydroxyapatite ceramics made of natural bone", Biomaterial, vol. 21, (2000) 1645-1658.

[104] D. J. A. Netz, P. Sepulveda, V. C. Pandolfelli, A. C. C. Spadro, J.B. Alencastre, M. V. L. B. Bentley, J. M. Marchetti , "Potential use of gelcasting hydroxyapatite porous ceramic as an implantable drug delivery system", Intesnational Journal of Pharmaceutics, vol. 213, (2001) 117-125.

[105] P. Sepulveda, "Gelcasting foams for porous ceramics", American Ceramic Society bulletin, vol. 76, (1997) 61-65.

[106] H. M. Rootare, R. G. Craig, "Chracterization of the compaction and sintering of hydroxyapatite powders by mercury porosimetry", Powder Technology, vol. 9, (1974) 199-211.

[107] H.M. Rootare, C.F. Prenzlow, "Surface areas from mercury porosimeter measuments", Journal of Physical Chemistry, vol. 71, (1967) 2733-2736.

[108] S. Brunauer, P.H. Emmett, E. Teller, "Adsorption of gases in multimolecular layers", Journal of American Chemical Societty, vol. 60, (1938) 309-319.

[109] I. H. Arita, D. S. Wilkinson, M. A. Mondragon, V. M. Castano, "Chemistry and sintering behaviour of thin hydroxyapatite ceramicss with controlled porosity", Biomaterials, vol. 16, (1995) 403-408.

[110] D. M. Liu, "Influence of porous microarchitecture on the in-vitro dissolution and biological behaviour of porous calcium phosphate ceramics", Meterial Science Forum, vol. 250, (1997) 183-208.

[111] V. Karageorgiou, D. Kaplan, "Porosity of 3D biomaterial scaffolds and osteogenesis", Biomaterials, vol. 26, (2005) 5474-5491.

[112] I. Sopyan, M. Mel, S. Ramesh, K. A. Khalid, "Porous hydroxyapatite for artificial bone applications", Science and Technology of Advanced Materials, vol. 8, (2007) 116-123.

[113] T.J.Webster, E.A. Massa-Schlueter, J.L.Smith, E.B. Slamovich, "Osteoblast response to hydroxyapatite doped with divalent and trivalent cations", Biomaterials, vol. 25, (2004) 2111-2121.

[114] B. Basar, A. Tezcaner, D. Keskin, Z. Evis, "Improvements in microstructural, mechanical, and biocompatibility properties of nano-sized hydroxyapatites doped with yttrium and fluoride", Ceramics International, vol. 36, (2010) 1633-1643.

[115] H. W. Kim, Y. J. Noh, Y. H. Koh, H. E. Kim, H. M. Kim, "Enhanced performance of fluorine substituted hydroxyapatite composites for hard tissue engineering", Journal of Material Science: Material in Medicine, vol. 14, (2003) 899-904.

[116] E. Jallot, J. M. Nedelec, A. S. Grimault, E. Chassot, A. Grandjean Laquerriere, P. Laquerriere, D. Laurent-Maquin, "STEM and EDXS characterisation of physico-chemical reactions at the periphery of sol–gel derived Zn-substituted hydroxyapatites during interactions with biological fluids", Colloids and Surfaces B: Biointerfaces, vol. 42, (2005) 205-210.

[117] J. Jang, S. Kim, "Factors affecting diametral tensile strength of microfilled dental composites", Polymer Journal, vol. 28, (1996) 293-298.

[118] Z. Evis, F. Ozturk, "Investigation of tensile strength of hydroxyapatite with various porosities by diametral strength test", Materials Science and Technology, vol. 24, (2008) 274-278.

[119] K.T. Chau, X.X. Wei, "A new analytic solution for the diametral point load strength on finite solid circular cylinders", International Journal of Solids and Structures, vol. 38, (2001) 1459-1481.

[120] A. Bigi, E. Foresti, R. Gregorini, A. Ripamonti, N. Roveri, J. S. Shah, "The role of magnesium on the structure of biological apatite", Calcified Tissue International, vol. 50, (1992) 439-444.

[121] V.S. Komlev, S.M. Barinov, F. Rustichelli, "Strength enhancement of porous hydroxyapatite ceramics by polymer impregnation", Journal of Materials Science Letters, vol. 22, (2003) 1215-1217.

[122] S. Best, W. Bonfield, C. Doyle, "In Proceedings of the Second International Symposium on Ceramics in Medicine", edited by Heimke G., Heidelberg, Germany, (1989) 57-64.

[123] C. Ergun, H. Liu, T. J. Webster, "Osteoblast adhesion on novel machinable calcium phosphate/lanthanum phosphate composites for orthopedic applications", Journal of Biomedical Materials Research. Part A, vol. 89, (2009) 727-733.

[124] C. Achilli, S. Grandi, A. Ciana, G. F. Guidetti, A. Malara, V. Abonante, L. Cansolino, C. Tomasi, A. Balduini, M. Canobbio, C. Balduini, G. Minetti, "Biocompatibility of functionalized boron phosphate nanoparticles for boron neutron capture therapy application", Nanomedicine: Nanotechnology, Biology and Medicine, vol. 10, (2014) 589-597.

[125] D. Chou, D. Hong, P. Saha, J. Ferrero, B. Lee, Z. Tan, Z. Dong, P. Kumta, "In vitro and in vivo corrosion, cytocompatibility and mechanical properties of biodegradable Mg-Y-Ca-Zr alloys as implant material", Acta Biomaterialia, vol. 9, (2013) 8518-8533.

[126] L. Horvath, A. Magrez, D. Golberg, C. Zhi, Y. Bando, R. Smajda, E. Horvath, L. Forro, B. Schwaller, "In vitro investigation of the cellular toxicity of boron nitride nanotubes", Journal of Biomedical Materials Research. Part A, vol. 5, (2011) 3800-3810.

[127] C. Ratisoontorn, M. L. Seto, K. M. Broughton, M. L. Cunningham, "In vitro differentiation profile of osteoblasts derived from patients with Saethre-Chotzen syndrome", Bone, vol. 36, (2005) 627-634.

[128] S. An, T. Matsumoto, H. Miyajima, A. Nakahira, K. Kim, S. Imazato, "Porous zirconia/hydroxyapatite scaffolds for bone reconstruction", Dental Materials, vol. 28, (2012) 1221-1231.

[129] Y. Li, C. Wen, D. Mushahary, R. Sravanthi, N. Harishankar, G. Pande, P. Hodgson, "Mg-Zr-Sr alloys as biodegradable implant materials", Acta Biomaterialia, vol. 8, (2012) 3177-3188.

[130] M. Sandhyrani, N. Rameshbabu, K. Venkateswarlu, L. Rama Krishna, "Fabrication, characterization and in-vitro evaluation of nanostructured zirconia/hydroxyapatite composite film on zirconium", Surface and Coatings Technology, vol. 238, (2014) 58-67.

[131] M. Benderdour, T. Bui-van, A. Dicko, F. Belleville, "In vivo and in vitro effects of boron and boronated compounds", Journal of Trace Elements in Medicine and Biology, vol. 12, (1998) 2-7.

[132] R. Quan, D. Yang, X. Wu, H. Wang, X. Miao, W.Li, "In vitro and in vivo biocompatibility of graded hydroxyapatite-zirconia composite bioceramic", Journal of Materials Science. Materials in Medicine, vol. 19, (2008) 3800-3810.

[133] M. A. F. Afzal, P. Kesrawani, K. M. Reddy, S. Kalmodia, B. Basu, K. Balani, "Functionally graded hydroxyapatite-alumina-zirconia biocomposite: Synergy of toughness and biocompatibility", Materials Science and Engineering C, vol. 32, (2012) 1164-1173.

APENDIX A.

1 way ANOVA-Tukey's multiple comparisons test results of pure HA and different composites on days 1 and 7

1 way ANOVA-Tukey's multiple comparisons test was conducted on the viability results obtained in this study. The objective is to compare the average viability of each composite with all others and also control groups which are pure HA and tissue culture flask (TCPS). For the sake of abbreviation, the samples of first group which includes zirconia are labeled G1 and four different composites of that group are labeled C1, 2, 3 and 4 respectively. The same abbreviated model is applied to composites of second group including boron oxide (G2).

In order to express the null and alternative hypothesis, columns are labeled with i and rows with j. The null and alternative hypothesis used in this analysis is then:

$$\forall\, i,j \qquad H_0 = \mu_i - \mu_j = 0$$

$$H_1 = \mu_i - \mu_j \neq 0$$

ANOVA is applied at a significance level of $\alpha=0.05$:

If $p<\alpha=0.05$; H_0 is rejected;

If $p\geq\alpha=0.05$; H_0 can not be rejected;

Which means if the p value calculated is higher value than α, then there is no statistically significant difference between the average of i and j, but if the p value is equal to or smaller than the significance level α, then there exists a statistically significant difference between i and j.

Table A1 - 1 way ANOVA-Tukey's multiple comparisons test results of pure HA and different composites on day 1. Data are depicted as Mean ± SEM (* p<0.05, ** p<0.005, *** p<0.0005, **** p<0.0001, NS = not significant).

	G1C1	G1C2	G1C3	G1C4	G2C1	G2C2	G2C3	G2C4	HA	TCPS
G1C1		NS	NS	NS	****	NS	****	NS	NS	NS
G1C2	NS		NS	NS	****	NS	****	NS	NS	NS
G1C3	NS	NS		NS	**	NS	*	NS	NS	*
G1C4	NS	NS	NS		*	NS	*	NS	NS	*
G2C1	****	****	**	*		***	NS	NS	****	****
G2C2	NS	NS	NS	NS	***		**	NS	NS	NS
G2C3	****	****	*	*	NS	**		NS	****	****
G2C4	NS	NS	NS	NS	NS	NS	NS		*	**
HA	NS	NS	NS	NS	****	NS	****	*		NS
TCPS	NS	NS	*	*	****	NS	****	**	NS	

Table A2 - 1 way ANOVA-Tukey's multiple comparisons test results of pure HA and different composites on day 3. Data are depicted as Mean ± SEM (* p<0.05, ** p<0.005, *** p<0.0005, **** p<0.0001, NS = not significant).

	G1C1	G1C2	G1C3	G1C4	G2C1	G2C2	G2C3	G2C4	HA	TCPS
G1C1		****	****	*	****	****	****	****	*	****
G1C2	****		****	****	****	NS	****	****	****	****
G1C3	****	****		****	****	****	NS	****	****	****
G1C4	*	****	****		****	****	****	****	NS	****
G2C1	****	****	****	****		****	**	****	****	****
G2C2	****	NS	****	****	****		****	***	****	****
G2C3	****	****	NS	****	**	****		****	****	****
G2C4	****	****	****	****	****	***	****		****	****
HA	*	****	****	NS	****	****	****	****		****
TCPS	****	****	****	****	****	****	****	****	****	

Table A3 - 1 way ANOVA-Tukey's multiple comparisons test results of pure HA and different composites on day 7. Data are depicted as Mean ± SEM (* $p<0.05$, ** $p<0.005$, *** $p<0.0005$, **** $p<0.0001$, NS = not significant).

	G1C1	G1C2	G1C3	G1C4	G2C1	G2C2	G2C3	G2C4	HA	TCPS
G1C1		NS	****	NS	****	**	****	****	NS	****
G1C2	NS		****	NS	****	**	****	****	NS	****
G1C3	****	****		****	NS	****	NS	NS	****	****
G1C4	NS	NS	****		****	****	****	****	NS	****
G2C1	****	****	NS	****		****	*	**	****	****
G2C2	**	**	****	****	****		****	****	****	****
G2C3	****	****	NS	****	*	****		NS	****	****
G2C4	****	****	NS	****	**	****	NS		****	****
HA	NS	NS	****	NS	****	****	****	****		****
TCPS	****	****	****	****	****	****	****	****	****	